Acta Neuropathologica (2019) 137:27–46
https://doi.org/10.1007/s00401-018-1942-8

ORIGINAL PAPER

Neurons selectively targeted in frontotemporal dementia reveal early stage TDP-43 pathobiology

Alissa L. Nana[1] · Manu Sidhu[1] · Stephanie E. Gaus[1] · Ji-Hye L. Hwang[1] · Libo Li[1,2] · Youngsoon Park[1] · Eun-Joo Kim[1] · Lorenzo Pasquini[1] · Isabel E. Allen[3] · Katherine P. Rankin[1] · Gianina Toller[1] · Joel H. Kramer[1] · Daniel H. Geschwind[4] · Giovanni Coppola[4] · Eric J. Huang[5] · Lea T. Grinberg[1,5,6] · Bruce L. Miller[1] · William W. Seeley[1,5]

Received: 31 August 2018 / Revised: 22 November 2018 / Accepted: 23 November 2018 / Published online: 3 December 2018

Abstract

TAR DNA-binding protein 43 (TDP-43) aggregation is the most common pathological hallmark in frontotemporal dementia (FTD) and characterizes nearly all patients with motor neuron disease (MND). The earliest stages of TDP-43 pathobiology are not well-characterized, and whether neurodegeneration results from TDP-43 loss-of-function or aggregation remains unclear. In the behavioral variant of FTD (bvFTD), patients undergo selective dropout of von Economo neurons (VENs) and fork cells within the frontoinsular (FI) and anterior cingulate cortices. Here, we examined TDP-43 pathobiology within these vulnerable neurons in the FI across a clinical spectrum including 17 patients with sporadic bvFTD, MND, or both. In an exploratory analysis based on our initial observations, we further assessed ten patients with *C9orf72*-associated bvFTD/MND. VENs and fork cells showed early, disproportionate TDP-43 aggregation that correlated with anatomical and clinical severity, including loss of emotional empathy. The presence of a TDP-43 inclusion was associated with striking nuclear and somatodendritic atrophy. An intriguing minority of neurons lacked detectable nuclear TDP-43 despite the apparent absence of a cytoplasmic TDP-43 inclusion. These cells showed neuronal atrophy comparable to inclusion-bearing neurons, suggesting that the loss of nuclear TDP-43 function promotes neurodegeneration, even when TDP-43 aggregation is inconspicuous or absent.

Keywords Frontotemporal dementia (FTD) · Amyotrophic lateral sclerosis (ALS) · TAR DNA-binding protein 43 (TDP-43) · *C9orf72* · Von Economo neuron (VEN) · Empathy

Introduction

Frontotemporal dementia (FTD) and motor neuron disease (MND) represent the endpoints of a clinicopathological continuum linked to TAR DNA-binding protein 43 (TDP-43) proteinopathy, which is found in more than 50% of patients with bvFTD and almost all patients with FTD-MND and ALS [52]. Within this spectrum, some patients present with FTD, others MND, and still others develop a blended syndrome (FTD-MND) [27]. TDP-43 is a DNA/RNA-binding protein [13] expressed in all healthy neurons; in FTD/MND, neuronal cytoplasmic TDP-43 aggregation is accompanied by a loss of normal nuclear TDP-43. This observation raises

Electronic supplementary material The online version of this article (https://doi.org/10.1007/s00401-018-1942-8) contains supplementary material, which is available to authorized users.

✉ William W. Seeley
bill.seeley@ucsf.edu

[1] Department of Neurology, UCSF Weill Institute for Neurosciences, University of California, San Francisco, San Francisco, CA, USA

[2] Department of Psychopharmacology, Qiqihar Medical University, Qiqihar, China

[3] Department of Epidemiology and Biostatistics, University of California, San Francisco, San Francisco, CA, USA

[4] Neurogenetics Program, Department of Neurology and Semel Institute for Neuroscience and Human Behavior, David Geffen School of Medicine, University of California Los Angeles, Los Angeles, CA, USA

[5] Department of Pathology and Laboratory Medicine, University of California, San Francisco, San Francisco, CA, USA

[6] Global Brain Health Institute, University of California, San Francisco, San Francisco, CA, USA

the question of which factor drives neurodegeneration: TDP-43 aggregate toxicity, loss of TDP-43 function, or both. Although model-based experiments have begun to inform this debate [5, 32, 77, 82, 84], there remains no consensus and yet little work has been done to address this question in human tissues.

In MND, degeneration targets the upper and lower motor neurons within the pyramidal motor system. In FTD, the vulnerable circuits and cell types have just begun to emerge within the past decade. In the behavioral variant (bvFTD), the most common FTD syndrome, early degeneration involves the anterior cingulate (ACC) and ventral anterior insular (i.e., frontoinsular, FI) cortices [8, 66, 87], regardless of the underlying pathological cause [54]. These regions serve as the cortical hubs of a large-scale "salience network" [67] critical for social–emotional–autonomic function and are home to the morphologically distinctive von Economo neurons (VENs) [68, 79] and fork cells [53]. We and others have shown that these large layer 5 projection neurons undergo early dropout in bvFTD [34, 63–65, 86], but, to date, no bvFTD study has assessed VEN and fork cell pathological changes, such as protein aggregation or neuronal atrophy, occurring prior to neuronal death.

In the present work, we sought to determine whether VEN and fork cell vulnerability in bvFTD due to FTLD-TDP is associated with early TDP-43 aggregation and whether aggregation relates to anatomical and clinical measures of disease severity. To pursue these goals, we studied patients across the bvFTD-MND spectrum, reasoning that patients with pure MND or early bvFTD-MND may represent an early or arrested stage of bvFTD progression. In the course of this work, we recognized an important minority of VENs, fork cells, and other neurons that lack detectable nuclear TDP-43 despite the apparent absence of a cytoplasmic inclusion. These neurons, here termed "nuclear TDP-43-depleted", have been recently noted in FTD and MND by our group and others [6, 7, 78], but they have yet to be systematically characterized. Therefore, we also studied the morphology of nuclear TDP-43-depleted and TDP-43 inclusion-bearing neurons to determine whether the reduction of nuclear TDP-43 alone is associated with neuronal degeneration.

Materials and methods

Human brain material and subjects

Post-mortem human brain tissue was obtained from the USCF Neurodegenerative Disease Brain Bank. Consent for brain donation was obtained from all subjects or their surrogates in accordance with the Declaration of Helsinki and the research was approved by the University of California, San Francisco Committee on Human Research. Depending on where the autopsy was performed, brains were immersion fixed whole in 10% buffered formalin or cut fresh into 1 cm thick coronal slices. For freshly cut brains, alternate slices were fixed for 48–72 h in 10% buffered formalin or frozen. Clinical diagnoses of bvFTD were made according to prevailing international consensus criteria at the time of assessment [51, 60]. Clinical diagnoses of ALS were made according to El Escorial Criteria [9, 10]. The presence of MND in patients with bvFTD was assessed by a neurologist based on the neurological examination, usually supported by electrodiagnostic testing, and was recorded prospectively in the Memory and Aging Center database. Neuropathological diagnoses were made following consensus diagnostic criteria [41, 42, 45–47] using previously described histological and immunohistochemical methods [34, 76]. Cases were selected based on clinical and neuropathological diagnoses and genetic analysis (Suppl. Figure 1). Patients were required to have (1) a primary clinical diagnosis of bvFTD, bvFTD-MND, or amyotrophic lateral sclerosis (ALS)/MND, and (2) a neuropathological diagnosis of FTLD-TDP, Type B or U, with or without MND, or ALS-TDP. Within the FTLD-TDP spectrum, Type B, characterized by speckled or dash-like neuronal cytoplasmic TDP-43 inclusions (NCIs), and an unclassifiable "Type U", with insufficient or atypical TDP-43 inclusions, are the most common subtypes in bvFTD ± MND [41]. We limited the analyses to these types (Suppl. Figure 1) to focus on a more homogeneous pathological substrate, allowing us to make better inferences about stage-wise and clinical symptom relationships. Exclusion criteria were presence of a disease-causing mutation other than a *C9orf72* expansion, Braak neurofibrillary tangle stage ≥ 4, transitional limbic or diffuse neocortical Lewy body disease, and a post-mortem interval > 48 h. Control subjects were individuals with no clinical history of neuropsychiatric disorder. Based on these criteria, we studied 39 subjects in total (see Tables 1, 2, and Suppl. Figure 1 for details). 17 patients across the bvFTD-MND spectrum with no known FTD-related mutation and primary TDP-43 pathology were studied, alongside 10 age- and sex- matched non-neurological controls. To enable blinded characterization of patients with and without the *C9orf72* expansion, we included an additional 10 patients (mean age 60, 2 females) with the expansion who met all other inclusion criteria. Two additional patients with *C9orf72* expansion were included for morphometric assessment only (Table 2). Anatomical disease stage was assessed using an FTD rating scale [8], as previously described. Anatomical staging of all patients was performed by a single blinded investigator (W.W.S).

Table 1 Subject demographics

	Controls	Sporadic bvFTD/MND	*C9orf72*-bvFTD/MND
N	10	17	10
Clinical diagnoses	NA	3 ALS, 1 MND, 2 bvFTD-ALS, 5 bvFTD-MND, 6 bvFTD	2 ALS, 5 bvFTD-MND, 3 bvFTD
Neuropathological diagnoses	NA	4 ALS-TDP; 2 FTLD-TDP-B, ALS; 8 FTLD-TDP-B, MND; 3 FTLD-TDP-B	1 ALS-TDP; 5 FTLD-TDP-B, MND; 3 FTLD-TDP-U, MND; 1 FTLD-TDP-U
Gender (M:F)	6:4	10:7	8:2
Age at death (years)	63.6 (9.8)	61.8 (7.4)	59.8 (3.4)
Symptom duration (years)	NA	5.2 (2.8)	7.1 (6.9)
PMI (h)	43.1 (38.2)	13.0 (10.2)	13.3 (6.3)
Broe stage; median (range)	NA	1 (0–2)	1 (0–2)
Brain weight (g)	1244 (151)	1284 (138)	1257 (172)
CDR total	NA	1.8 (1.1)	1.3 (0.9)
CDR, sum of boxes	NA	8.9 (5.2)	7.5 (5.0)
Worst NPI, sum of apathy, disinhibition, motor, eating	NA	41.9 (25.1)	44.3 (27.5)
IRI, empathic concern subscale	NA	20.0 (8.0)	17.6 (7.3)

Unless otherwise noted, numbers in parentheses are SD of preceding mean

Clinical and behavioral assessment

Symptom duration was estimated from the clinical records. Clinical measures were obtained as previously described [34]. Briefly, clinical severity was assessed using the Clinical Dementia Rating (CDR) scale total and Sum of Boxes scores (CDR-SB), using a version of the CDR adapted for FTD [35]. In addition, we chose a validated measure of emotional empathy, the empathic concern subscale of the interpersonal reactivity index (IRI) [17], as completed by the patient's informant. Loss of empathy is a core diagnostic feature of bvFTD, and empathic concern deficits in bvFTD are related to degeneration of anterior insula, anterior cingulate/medial prefrontal, and anterior temporal regions involved in bvFTD [59, 69].

Specimens and tissue processing

Blocks of FI were dissected from ~ 1 cm thick formalin-fixed coronal slabs (right, left or bilateral, as available, see Table 2 for details) and stored until processed for sectioning and immunohistochemistry. Blocks were removed from storage in formalin or PBS with 0.02% sodium azide (PBS-Az) and cryoprotected in graded sucrose solutions (10, 20 and 30% sucrose in PBS-Az) then sectioned at 50 µm thickness on a freezing microtome. Every 12th section was Nissl-stained with cresyl violet (FD Neurotech) for neuron counts and to determine the anatomical boundaries of the FI, the cortical region of interest.

Immunohistochemistry

Three sections were selected from each block for immunohistochemical staining. Prior to staining, all sections were coded for rater blinding. Free-floating sections were washed (6 × 10 min) in 0.01 M phosphate-buffered saline and underwent antigen retrieval in 10 mM citrate buffer pH 6.0 for 2 h in an 80 °C water bath. Endogenous peroxidase activity was quenched with 3% hydrogen peroxide in PBS-Az for 30 min. Sections were then washed (3 × 10 min) in PBS and non-specific staining was blocked by incubating in 5% nonfat milk powder (Carnation) in PBS + 0.25% Triton X-100 (PBT) for 1 h. For TDP-43 immunostaining, sections were incubated with an antibody against TDP-43 (rabbit polyclonal, 1:5000, Proteintech, RRID: AB_615042) in PBT-Az with gentle agitation (orbital shaker) overnight at room temperature. Following incubation with primary antibody, sections were washed (6 × 10 min) in PBS, incubated for 1 h in biotinylated secondary antibody (goat anti-rabbit IgG, 1:500 in PBT, Vector), washed in PBS, incubated for 1 h in ABC (Vectastain ABC elite kit, Vector Laboratories, 1:500 each in PBS), washed, then exposed to 0.05% 3,3-diaminobenzidine tetrahydrochloride (Sigma) and 0.01% H_2O_2 to produce a brown reaction product. The sections were washed and mounted onto plus slides. Finally, sections were dehydrated through a graded ethanol series, cleared in xylene, and coverslipped with Permaslip. TDP-43 stained sections were counterstained with hematoxylin (Fisher).

Table 2 Detailed subject characteristics

Case no.	Age	Sex	Clinical diagnosis	Primary neuropathological diagnosis[a]	Side studied	Sx dur (years)	Broe stage	Thal phase	Braak stage	CERAD score	ADNC	CDR, sum of boxes	IRI—empathic concern
N1	46	F	NC	N/A	R & L	NA	ND	ND	ND	ND	ND	ND	ND
N2[b]	57	M	NC	N/A	R & L	NA	ND	ND	ND	ND	ND	ND	ND
N3	59	F	NC	N/A	R & L	NA	ND	ND	ND	ND	ND	ND	ND
N4	76	M	NC	N/A	R & L	NA	ND	1	2	Sparse	Low	ND	ND
N5	73	M	NC	N/A	R & L	NA	ND	0	1	Absent	Not	ND	ND
N6[b]	55	F	NC	N/A	R & L	NA	ND	0	0	Absent	Not	ND	ND
N7	72	F	NC	N/A	R & L	NA	ND	4	4	Frequent	Int.	ND	ND
N8	73	M	NC	N/A	R & L	NA	ND	2	2	Absent	Low	ND	ND
N9[b]	64	M	NC	N/A	R & L	NA	ND	0	1	Absent	Not	ND	ND
N10[b]	61	M	NC	N/A	R & L	NA	ND	1	1	Absent	Low	ND	ND
S1	49	M	ALS	ALS-TDP	R & L	3	0	1	0	Absent	Low	3	ND
S2	64	M	ALS	ALS-TDP	R & L	9	1	0	0	Absent	Not	ND	ND
S3	52	M	MND	ALS-TDP	R & L	7	0	0	1	Absent	Not	0	31
S4	67	F	ALS	ALS-TDP	R & L	2	1	4	2	Frequent	Low	0	ND
S5[b]	51	F	bvFTD-MND	FTLD-TDP-B; MND	R & L	3	1	2	0	Absent	Low	11	31
S6	58	F	bvFTD-MND	FTLD-TDP-B; MND	R & L	3	1	1	0	Absent	Low	11	23
S7	66	M	bvFTD-MND	FTLD-TDP-B, MND	L	3	2	2	2	Absent	Low	9	20
S8	72	M	bvFTD-MND	FTLD-TDP-B	R & L	1	0	0	4	Absent	Not	18	ND
S9[b]	60	M	bvFTD-ALS	FTLD-TDP-B, ALS	R	7	1	3	1	Frequent	Low	10	23
S10[b]	65	M	bvFTD-MND	FTLD-TDP-B, MND	R & L	5	0	1	1	Sparse	Low	10	9
S11[b]	64	M	bvFTD-ALS	FTLD-TDP-B, MND	R	9	0	1	1	Absent	Low	5.5	20
S12	53	F	bvFTD	FTLD-TDP-B	R & L	6	1	0	0	Absent	Not	13	ND
S13	75	F	bvFTD	FTLD-TDP-B; MND	R & L	3	0	3	4	Absent	Int.	9	19
S14[b]	66	M	bvFTD	FTLD-TDP-B, MND	R	8	2	2	2	Sparse	Low	5.5	ND
S15	65	F	bvFTD	FTLD-TDP-B, MND	R	9	1	1	2	Absent	Low	15	12
S16[b]	57	F	bvFTD	FTLD-TDP-B, ALS	R	3	2	0	0	Absent	Not	7	25
S17[b]	66	M	bvFTD	FTLD-TDP-B	R	8	1	2	2	Moderate	Low	15	7
C1[b]	62	F	ALS	FTLD-TDP-B, MND	R & L	2	0	0	1	Absent	Not	4	30
C2[b]	58	M	ALS	ALS-TDP	R	2	1	1	2	Absent	Low	0	28
C3	59	M	bvFTD-MND	FTLD-TDP-U, MND	L	7	0	2	2	Absent	Low	5	18
C4	57	M	bvFTD-MND	FTLD-TDP-B; MND	R & L	1	0	1–2	0	Absent	Low	7	19
C5[b]	59	M	bvFTD-MND	FTLD-TDP-B; MND	L	9	2	0	0	Absent	Not	6	14
C6	58	M	bvFTD-MND	FTLD-TDP-U, MND	R	3	1	2	1	Sparse	Low	3.5	ND
C7[b]	56	M	bvFTD-MND	FTLD-TDP-U, MND	R	14	2	1	1	Absent	Low	8	15
C8[b]	67	M	bvFTD	FTLD-TDP-B; MND	R	23	1	3	3	Sparse	Int.	16	15
C9	65	F	bvFTD	FTLD-TDP-U	R	8	1	1	3	Absent	Low	15	9

Table 2 (continued)

Case no.	Age	Sex	Clinical diagnosis	Primary neuropathological diagnosis[a]	Side studied	Sx dur (years)	Broe stage	Thal phase	Braak stage	CERAD score	ADNC	CDR, sum of boxes	IRI—empathic concern
C10	57	M	bvFTD	FTLD-TDP-B, MND	L	2	0	1	0	Absent	Low	10	10
C11[c]	59	M	bvFTD-MND	ALS-TDP	R	12	ND	1	1	Absent	Low	8	ND
C12[c]	60	F	bvFTD-MND	FTLD-TDP-B, MND	R	17	1	1	4	Absent	Low	10	ND

NC neurologically unaffected control, *S* sporadic disease, *C C9orf72*-associated disease, *N/A* not applicable, *R* right, *L* left, *ND* not done

[a]The diagnosis thought most likely to have caused the clinical syndrome; *Sx dur* symptom duration; *ADNC* Alzheimer's disease neuropathologic change

[b]Subject included in inclusion fraction and morphometry studies

[c]Subject included in morphometry study only

Immunofluorescence staining and confocal imaging

Multiple immunofluorescence staining was used to further characterize TDP-43 inclusions. Five-color immunofluorescence labeling was performed using fluorescent Nissl to label nuclei, anti-MAP2 (chicken polyclonal, 1:3000, EnCor Biotechnology Inc., RRID: AB_2138173) to label neuronal somata and proximal dendrites, a pan TDP-43 antibody (mouse monoclonal, 1:30,000, Proteintech, RRID: AB_2200520) to label physiological (nuclear) TDP-43 and TDP-43 inclusions, phosphorylated TDP-43 (rat monoclonal, 1:500, courtesy Manuela Neumann, RRID: AB_2315226), and ubiquitin (rabbit polyclonal, 1:500, DAKO, RRID: AB_2315524) antibodies. Sections were initially photobleached to reduce autofluorescence. Free-floating tissue sections were immersed in PBS-Az, carefully positioned to lay flat, and photobleached for 72 h at 4 °C using a 240 W wide-spectrum light (HTG Supply LED-6B240) with an array of 80 3 W LEDs emitting at 6 bands: 390 nm, 430 nm, 460 nm, 660 nm, 630 nm and 1000 K white/blue light. Sections were then processed for antigen retrieval, blocked, and incubated with the first batch of primary antibodies (anti TDP-43 and anti-MAP2) overnight at room temperature. The next day, sections were washed, incubated with secondary antibodies conjugated to either a fluorescent dye or biotin, washed, then incubated with streptavidin-conjugated pacific orange. The tissue was then sequentially labeled with the second batch of primary antibodies (anti-phosphorylated TDP-43 and anti-ubiquitin), washed, again incubated with the appropriate Alexa Fluor-conjugated antibodies, counterstained with Neurotrace blue fluorescent Nissl, mounted onto slides, and dried. Sections were finally incubated with 0.01% Sudan black B to further reduce autofluorescence and coverslipped using Fluoromount G (Southern Biotech). Sections were imaged using a Zeiss LSM 880 confocal laser scanning microscope equipped with 405 (to image blue fluorescent Nissl, and pacific orange), 488 (Alexa Fluor 488), 561 (Alexa Fluor 568), and 633 (Alexa Fluor 647) lasers, and a filterless detection system with customizable emission bandwidths, enabling five channels to be imaged without spectral overlap.

ROI definition, image acquisition, and neuron quantification

Layer 5 of area FI was defined as previously described [34]. The extent of the agranular, VEN- and fork cell-containing FI was determined in cresyl violet-stained slides, and FI layer 5 and adjacent layers 2–3 were traced using Stereo Investigator (MBF Bioscience; system includes motorized stage and Nikon 80i microscope), mainly using an objective with 10× magnification. To obtain systematic, unbiased neuron counts, we used Stereo Investigator's Optical

Fractionator probe, in which neurons with nucleoli contained within a three-dimensional counting frame (or crossing the inclusion lines) were counted. Limited tissue availability prevented analysis of the entire FI; thus we did not aim to obtain stereological estimates of the entire population of FI neurons. VEN and fork cell densities and inclusion fractions were assessed in approximately 700 sampling sites, determined by our previous study [34] and pilot data to be sufficient to achieve a coefficient of error of ~ 0.1, from three sections spread out across the entire available FI (see Suppl. Tables 1 and 2 for details). Because VENs and fork cells were counted in the same counting frame, we based the number of sampling sites on the number required to achieve a coefficient of error ~ 0.1 for VENs, and some of the coefficients of error for fork cell density were greater than 0.1. Because neighboring layer 5 and layer 2–3 neurons are far more abundant, approximately 50–70 frames were counted per subject to assess these neuron densities and inclusion fractions. Nissl-based neuronal density estimates from subjects N1–N3, S1–S4, and C3 have been published previously [34] and are included in the present study for completeness of the neuronal loss data set. VEN, fork cell, and neighboring neuron loss in layer 5 of the FI was assessed in Nissl-stained sections from patients and controls with a 60×, N.A. 1.4 oil immersion objective. We similarly assessed the proportion of each cell type with TDP-43 inclusions among total layer 5 VENs, forks, and neighboring layer 5 neurons and layer 2–3 neurons, but used digitized "virtual" sections for improved workflow and blue/brown color discrimination. To this end, we scanned TDP-43 immunostained sections adjacent to each Nissl-stained sections; for each section, the regions of interest (FI layer 5 and layer 2–3) were traced in Stereo Investigator and exported into Zen software (Zeiss). An AxioObserver Z1 microscope (Zeiss) equipped with a motorized stage was used to acquire and montage digital, high magnification (63×, N.A. 1.4 oil immersion objective), image stacks (z-stack interval: 0.4 µm) of the entire FI Layer 5. Stitched montages were saved as Zeiss CZI images, exported as TIFF files, then compressed to create virtual JPX files for viewing in Stereo Investigator. The numbers of VENs, fork cells, neighboring layer 5 neurons, and layer 2–3 neurons with and without TDP-43 inclusions were then counted to obtain the percentage of inclusion-bearing neurons (i.e. "inclusion fraction" in each population. While counting, we also noted all neurons that showed loss of nuclear TDP-43 in the absence of a visible cytoplasmic inclusion ("nuclear TDP-43-depleted" neurons).

Cortical thickness measurements

Because apparent local density measurements can be artificially inflated by tissue volume loss, we measured cortical thickness in FI to estimate overall degeneration. Cortical boundaries of the agranular, VEN- and fork cell-containing FI were traced using Stereo Investigator software on cresyl violet-stained sections by following the superficial border of Layer 1 and the deep border of Layer 6 where it meets the white matter. The shortest distance between the traced Layer 1 and Layer 6 borders was measured at five points evenly spaced throughout the traced region of interest. Sulci and obliquely cut regions were excluded.

Inter-rater and intra-rater comparisons

To obtain layer 5 VEN/total neuron and fork cell/total neuron ratios, and VEN, fork cell and neighboring layer 5 neuron densities, three blinded raters (E.J.K, L.L. and Y.P) performed counting of Nissl-stained sections after training to predefined competency criteria, as described [34], which are designed to promote inter-rater consistency. Intra-rater reliability was assessed independently by each rater every 12 sections. Six sections were recounted by each Nissl rater for intra-class correlation analysis. Intra-rater correlation coefficients across the three raters averaged 0.990 (95% CI 0.923–0.999) for VENs, 0.995 (95% CI 0.959–0.999) for fork cells, and 0.987 (95% CI 0.901–0.999) for neighboring layer 5 neurons.

To assess TDP-43 inclusions and depletion in VENs, fork cells and neighboring layer 5 neurons, three blinded raters (S.E.G., A.L.N., and J.H.H.) performed counting of TDP-43 stained sections after training to predefined competency criteria. For TDP-43 inclusion counts, competency was defined as VEN, fork, and neighboring layer 5 neuron numbers, as well as ratio of affected/total neurons for each cell type, within 10% of values generated for a training section counted by a senior investigator (W.W.S.). Intra-rater reliability was assessed independently by each rater every six sections for a total of six sections per rater. Intra-class correlation coefficients for intra-rater reliability of inclusion fraction measurements were high, averaging 0.973 (95% CI 0.905–0.993) for VENs, 0.997 (95% CI 0.988–0.999) for fork cells, 0.978 (95% CI 0.840–0.998) for neighboring layer 5 neurons, and 0.998 (95% CI 0.985–1.000) for layer 2–3 neurons across raters.

Morphometry

Cell type-tailored neuronal morphology was assessed in a subset of age- and sex-matched subjects (seven sporadic bvFTD ± MND, two *C9orf72*-ALS, five *C9orf72*-bvFTD ± MND, and four controls, see Table 2 for subject details and Suppl. Table 3 for group demographics) selected because their tissue fixation was long-term, ideal for a detailed morphometric study. In studying all subjects with suitable tissue, two subjects were included in the *C9orf72* group that had not been included in the blinded *C9orf72* cohort for

density or inclusion fraction analysis. Control subjects were included to determine whether inclusion-lacking neurons in patients were altered compared with neurons in controls. Using Stereo Investigator and the same digitized slides used for TDP-43 counts, we manually measured apical and basal dendritic diameter and nuclear and somatic area (Suppl. Figure 2) in selected VENs, fork cells, and neighboring layer 5 neurons. TDP-43 normal cells were selected in a single section by systematic random sampling of layer 5 to yield a total of ten neurons per subject. For identification of neurons with TDP-43 neuronal cytoplasmic inclusions (NCIs) or TDP-43 nuclear depletion without NCIs, layer 5 of a single section was exhaustively scanned using the meander scan function in Stereo Investigator. If the exhaustive search of layer 5 of a single section yielded less than ten neurons of each cell type per group, additional sections were added until at least ten neurons were identified in each group, or until all three TDP-43 stained virtual sections had been exhaustively searched. If more than ten neurons per cell type per cell type and group were identified, excess neurons were randomly eliminated. Because neurons with TDP-43 nuclear depletion without an NCI were the rarest group, all identified neurons in this category were included for analysis. Nuclear and somatic areas were obtained by focusing through the cell and tracing the outline of the nucleus or soma at the widest part of the neuron. Apical and basal dendritic widths were measured at the maximum width of the dendrite at the junction between the soma and dendrite. For fork cells, the width of both apical dendrites was measured and the results averaged to yield one apical dendrite measurement per neuron. For pyramidal cells the width of the largest visible basal dendrite was measured.

Statistical analysis

Statistical analysis was performed using R version 3.4.3 in RStudio 1.1.383. Normality was assessed using parametric Q–Q plots and the Shapiro–Wilk normality test. Neuronal loss, inclusion fractions, and morphometry data were assessed using linear mixed-effects models using the R function "lmer" in the lme4 package (http://www.r-project.org). For all models, the only random effect in the model was subject-specific random intercepts, with all other effects considered as fixed. To examine whether there were significant differences in cell loss between patients with sporadic disease and controls, we used linear mixed-effects models with log-transformed neuronal density or fraction of total neurons as outcomes and clinical diagnosis as a primary categorical predictor with cerebral hemisphere and cortical thickness as covariates. To assess differences in TDP-43 inclusion fraction or TDP-43 depletion between cell types, we used a linear mixed-effects model with inclusion fraction as the outcome and cell type as a primary categorical predictor with hemisphere, Broe stage, and clinical diagnosis as covariates. To investigate whether VEN, fork cell, or neighboring layer 5 neuron density was altered in patients with a *C9orf72* mutation, we used a linear mixed-effects model with neuronal density as the outcome and clinical diagnosis as a primary categorical predictor with cerebral hemisphere, cortical thickness, and *C9orf72* status as covariates. TDP-43 inclusion fraction and TDP-43 depletion in *C9orf72* bvFTD/MND were assessed using the linear mixed-effects model described above for sporadic bvFTD/MND but with *C9orf72* status as an additional fixed effect. The effect of TDP-43 inclusions on cell morphology was tested with logistic mixed-effects models with each morphometric parameter as an outcome, TDP-43 status as the primary categorical predictor, and *C9orf72* status and clinical diagnosis as covariates. Normality of residuals was assessed for each model using a Q–Q plot and followed a normal distribution. For models assessing differences in percentages of each neuronal type with TDP-43 inclusions or depletion, residuals following a near normal distribution were accepted without log transforming the data. Normal approximations were used to find p values for mixed-effect models. A $p < 0.05$ (two-tailed) was considered significant. Significant interactions were further explored using the lsmeans package in *R*; p values for pairwise comparisons were adjusted using the Tukey method for multiple comparisons. Correlations between inclusion fractions and clinical and behavioral measures were assessed by Spearman partial correlation. Because clinical and behavioral measures were taken at a range of intervals prior to death, we controlled for time between clinical assessment and death, with the assumption that neuropathological features progress linearly over time.

K-means clustering [39], a nonhierarchical clustering method, was used in this study to obtain class memberships for the measured cells. K-means uses an iterative algorithm to update randomly selected initial cluster centers and to obtain cluster membership for each object, assuming defined boundaries between clusters. Initially, objects are assigned to a cluster on the basis of a minimal distance value. Next, centroids of the clusters are calculated and distance values between the centroids and each of the objects are recalculated. If the closest centroid is not associated with the cluster to which the object currently belongs, the object will switch its cluster membership to the cluster with the closest centroid. The centroid's positions are recalculated every time a component has changed its cluster membership. This process continues until none of the objects has been reassigned using the squared Euclidean distance metric [36, 44]. In this study, measured VENs were classified into three clusters, based on their nucleus and soma areas, and apical and basal dendritic diameters. A setting of 100 iterations and 10 replications was applied. K-means clustering was performed in MATLAB R2017a (https://www.mathworks.com/products/matlab.html) using the K-means function. The cross-tabulation

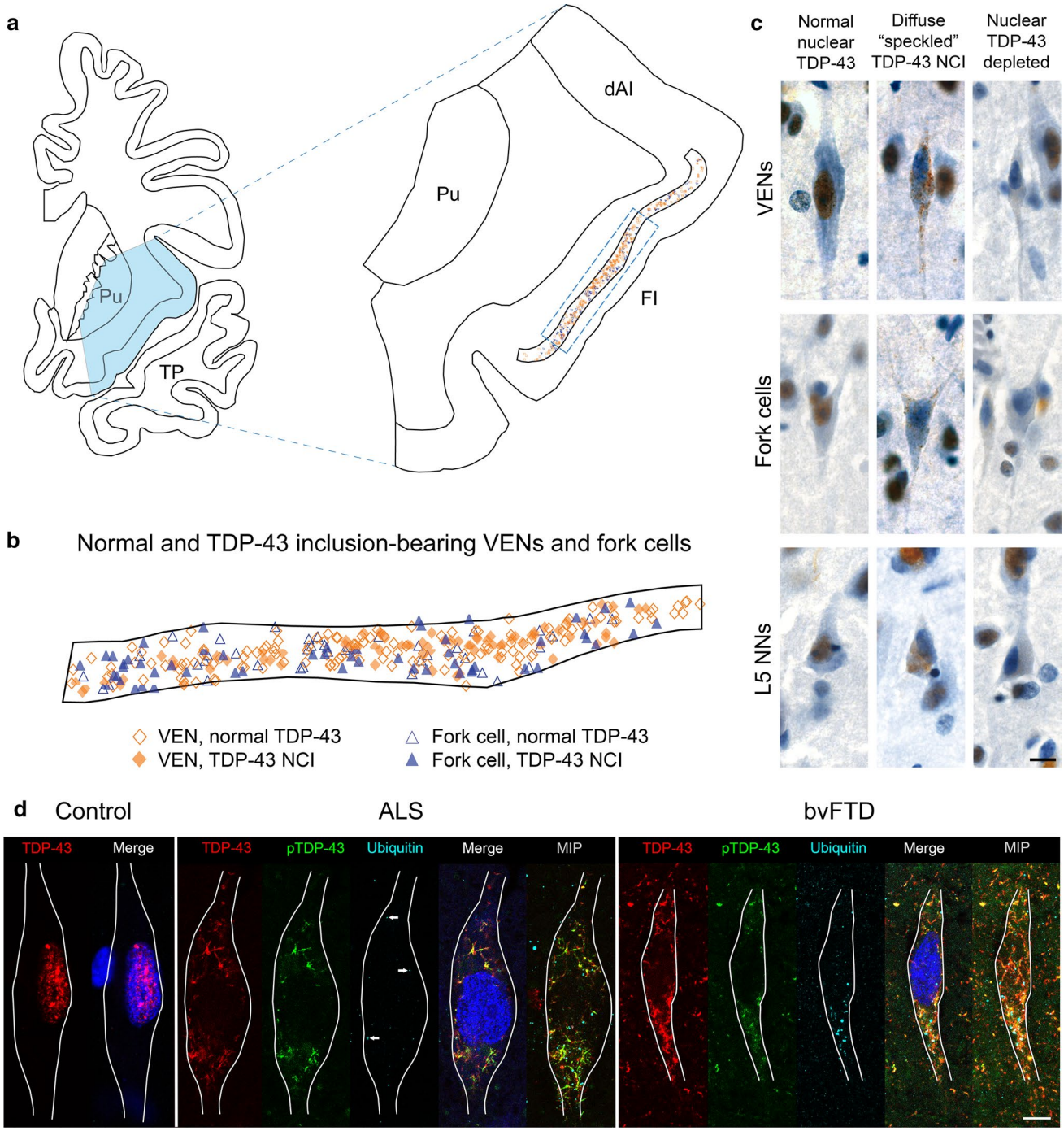

function in MATLAB was used to determine whether VENs were unevenly distributed across clusters by TDP-43 status.

To explore how each neuronal compartment (i.e., soma, nucleus, or apical or basal dendrite) was affected by TDP-43 aggregation or depletion, morphometric data for each compartment were transformed into z scores referenced to data from that compartment in neurons from control subjects. Z scores for each neuron were then ranked from highest to lowest, with VENs, fork cells, and neighboring layer 5 neurons assessed separately. A Chi square test was performed in RStudio to determine whether there was a relationship between TDP-43 inclusion/depletion status and compartment rank for each neuronal type, followed by pairwise comparisons between compartments corrected for multiple comparisons using false discovery rate.

◂**Fig. 1** Distribution of normal and inclusion-bearing neurons and patterns of TDP-43 aggregation in VENs, fork cells, and neighboring layer 5 neurons. **a**, **b** Mapping of all VENs and fork cells located in a section of the FI (outlined in **a**) in subject S5 shows similar distribution of normal and inclusion-bearing VENs and fork cells across layer 5 (**b**). B shows an expanded region of the FI indicated by the dashed rectangle in (**a**). **c** Punctate TDP-43 neuronal cytoplasmic inclusions (NCIs) were the most common inclusion type in VENs, fork cells, and neighboring layer 5 neurons (L5 NNs). Neurons without TDP-43 NCIs but lacking normal nuclear TDP-43 ("nuclear TDP-43-depleted") were observed for all cell types in the majority of patients. All images in (**c**) are from subject S5. **d** Images of VENs from a single confocal z slice with TDP-43 (red), phospho-TDP-43 (pTDP-43, green) and ubiquitin (cyan) immunostaining, and Nissl-stained nuclei (blue). MAP2 immunostaining (not shown) was used to trace VEN outlines. Normal VENs in control subjects (a VEN from subject N4 is shown) and patients with bvFTD/MND showed robust nuclear TDP-43 staining and no TDP-43 aggregation, phosphorylated TDP-43, or ubiquitin staining. In subjects with ALS (subject S4 is shown), TDP-43 inclusions were phosphorylated, with punctate, scattered ubiquitin staining dispersed around the TDP-43 inclusions. A few characteristic ubiquitin puncta are indicated by arrows on the single z slice from the patient with ALS, and are more clearly seen on a maximum intensity projection of 15 z slices through the VEN soma. In severely affected subjects (subject S15 is shown), TDP-43 inclusions were phosphorylated and foci of ubiquitination were larger and more numerous. The merge of red (TDP-43) and green (phospho-TDP-43) is shown as yellow. Brightness and contrast for each color channel in D were adjusted separately. Scale bars in (**c**) and (**d**) represent 10 µm. *dAI* dorsal anterior insula, *FI* frontoinsular cortex, *MIP* maximum intensity projection, *Pu* putamen, *TP* temporal pole

Results

To gain novel insights into TDP-43 pathobiology in humans, we sought to evaluate the earliest clinical stages of sporadic bvFTD, focusing on neuronal populations known to undergo early, selective degeneration. We included patients with ALS having no or few behavioral changes, those with mild bvFTD who developed and died of MND, and those with a full-blown bvFTD syndrome, with or without MND. Although bvFTD can result from the full FTLD pathological spectrum, including FTLD-tau or -FUS, here we included only patients with underlying FTLD-TDP or ALS-TDP.

Cortical atrophy, thinning, and neuronal density in the sporadic bvFTD-MND spectrum

To confirm that our cohort represented a range of stages beginning with limited neuronal loss, we assessed atrophy severity according to a staging system developed for bvFTD [8]. Patients were scored as having no atrophy (stage 0, $n=6$), very mild atrophy (stage 1, $n=8$), or mild atrophy (stage 2, $n=3$). No patient had moderate (stage 3) or severe (stage 4) atrophy. As expected, cortical thickness decreased with progressive Broe stage (Suppl. Figure 3a) and was therefore incorporated into statistical models to adjust for neuronal density increase that result from cortical thinning.

As anticipated, frontoinsular VEN and fork cells showed only mild, statistically non-significant reductions in neuronal density (VENs, 32% loss, $t=-1.87$, $p=0.061$; fork cells, 24% loss, $t=-1.70$, $p=0.089$; Suppl. Figure 3b). VEN and fork cell counts as a proportion of total layer 5 neurons showed similar findings (Suppl. Figure 3c). Neighboring layer 5 neurons (Suppl. Figure 3b) showed normal densities ($t=1.43$, $p=0.15$). Laterality had no significant effect on neuronal density. Thus, our diverse patient cohort, ranging in clinical presentation from pure ALS to pure bvFTD, represents an earlier stage of VEN and fork cell degeneration than reported in our previous smaller study of bvFTD due to FTLD-TDP, FTLD-tau, or FTLD-FUS, in which we observed 53% VEN and 68% fork cell loss in FI [34]. Grouping neuron loss by Broe stage (Suppl. Figure 3d) or clinical diagnosis (Suppl. Figure 3e) suggested progressive VEN and fork cell loss with advancing severity, with 40–50% loss by Broe stage 1 (Suppl. Figure 3d). An apparent increase in the ratio of VENs and fork cells to neighboring layer 5 neurons at Broe stage 2 likely reflected pyramidal neuron dropout as the disease progresses.

Von Economo neurons and fork cells show early, disproportionate TDP-43 aggregation in the sporadic bvFTD-MND spectrum

Having established that our study represents a range of neurodegeneration severities starting from no or minimal neuronal loss, we asked whether and at what stage VENs and fork cells undergo TDP-43 inclusion formation. Visual review of the materials suggested a striking propensity of VENs and fork cells to form TDP-43 neuronal cytoplasmic inclusions in comparison with neighboring Layer 5 neurons. An exhaustive map of an FI section from a representative patient with bvFTD-ALS at Broe stage 1 (Fig. 1a) reveals the distribution of normal and TDP-43 inclusion-bearing VENs and fork cells, which were distributed throughout layer 5 (Fig. 1a, b). VENs and fork cells most frequently presented with punctate/diffuse "speckled" or dash-like TDP-43 neuronal cytoplasmic inclusions typical of FTLD-TDP, Type B (Fig. 1c). To characterize the post-translational modifications of the characteristic "speckled" TDP-43 inclusions in VENs and fork cells, we performed multiple immunofluorescence labeling for TDP-43, phosphorylated TDP-43, and ubiquitin (Fig. 1d). In patients with ALS, the VEN and fork cell TDP-43 inclusions adopted dash-like or reticular, mesh-like structures in the cytoplasm; these deposits were almost always phosphorylated, at least in part, with sparse, punctate ubiquitin labeling across the TDP-43 mesh-like structure. In patients with bvFTD, VEN inclusions were also reticular and phosphorylated but contained larger, more globular areas of ubiquitination not part of the mesh-like TDP-43 inclusion structure. We did not observe VENs with phosphorylated

TDP-43-positive inclusions that were stained negatively using the pan TDP-43 antibody. To our initial surprise, but in keeping with recent studies from our group [78] and others [6, 7], we also observed neurons lacking normal nuclear TDP-43 despite the absence of any visible cytoplasmic inclusion on brightfield imaging (Fig. 1c). Although no TDP-43 inclusions were identified in these neurons, they may contain small amounts of cytoplasmic TDP-43 below the detection threshold of our antibody, but the degree of nuclear TDP-43 depletion was unambiguous in comparison to other neurons in the same patient or in controls.

Systematic, unbiased counting confirmed that, despite the mild neuronal loss, VENs ($t = 8.20$, $p < 0.0001$) and fork cells ($t = 8.98$, $p < 0.0001$) were three to fivefold more prone to TDP-43 inclusion formation than were neighboring layer 5 neurons (Fig. 2a). This effect was observed in both the left and right FI (inclusion fractions, left: VENs, 25%; fork cells, 28%; neighboring layer 5 neurons, 6%; inclusion fractions, right: VENs, 26%; fork cells, 26%; neighboring layer 5 neurons, 8%) (Fig. 2a and Suppl. Figure 4a). Nuclear TDP-43-depleted neurons showed the same selectivity pattern across cell types (Fig. 2b), with significantly higher rates of nuclear TDP-43 depletion found in VENs ($t = 4.14$, $p < 0.0001$) and fork cells ($t = 4.48$, $p < 0.0001$) than in neighboring layer 5 neurons, although rates of nuclear TDP-43 depletion were generally low and varied between subjects (Suppl. Figure 4a). Consistent with our current and previous [34] studies of FI VEN and fork cell loss, which showed no distinct hemispheric pattern, we saw no consistent difference in inclusion fraction between left and right FI ($t = -1.20$, $p = 0.23$) in the ten patients for whom bilateral FI was available. Some showed right-predominant, others left-predominant, and the remainder symmetrical TDP-43 inclusion formation rates (Suppl. Figure 4b).

Superficial cortical layers show prominent neuropil degeneration [11, 12] and inclusion burden [14, 40, 62] in FTLD-TDP. We therefore compared inclusion burden in FI layer 2–3 neurons to that seen in FI layer 5 neurons. Layer 2–3 neurons were significantly more prone to TDP-43 inclusions (left, 21%; right, 22%, $t = 6.42$, $p < 0.0001$) compared with layer 5 non-VEN, non-fork neurons (i.e., neighboring layer 5 neurons), yet showed a slightly lower inclusion fraction than VENs and fork cells in absolute terms (Fig. 2a). Nuclear TDP-43-depleted neuron fractions, however, were significantly higher in VENs ($t = 2.64$, $p = 0.0083$) and fork cells ($t = 2.98$, $p = 0.0029$) than in layer 2–3 neurons (Fig. 2b). Nuclear TDP-43-depleted neuron fractions did not differ significantly between layer 2–3 and neighboring layer 5 neurons ($t = -1.45$, $p = 0.15$).

Despite the absence of gross atrophy, cortical thinning, and significant overall neuronal loss at Broe stage 0, 18% of FI VENs and 20% of fork cells, but only 5% of neighboring layer 5 neurons, showed TDP-43 aggregation (Fig. 2c). Layer 2–3 neurons (13% inclusion fraction) fell midway between VENs/fork cells and neighboring layer 5 neurons. Patients with a more advanced disease stage (stages 1–2) showed a trend toward a higher proportion of neurons with TDP-43 inclusions across cell types, with the gap between VENs/fork cells and layer 2–3 neurons narrowing at stage 1 and closing by stage 2 (Fig. 2c). In contrast, the rate of nuclear TDP-43 depletion was similar in VENs, fork cells, and layer 2–3 neurons at Broe stage 0, although nuclear TDP-43 depletion was more prominent in VENs and fork cells than neighboring layer 5 neurons and layer 2–3 neurons at Broe stages 1 and 2 (Fig. 2d). Due to substantial inter-subject variability, however, the interaction between Broe stage and neuron type was not significant for TDP-43 inclusions ($F = 1.49$, $p > 0.1$) or nuclear depletion ($F = 1.54$, $p > 0.1$).

VEN and fork cell TDP-43 inclusion fraction relates to clinical diagnosis, overall symptom severity, and loss of emotional empathy in the sporadic bvFTD/MND spectrum

Patients with bvFTD develop progressive social–emotional deficits that undermine day-to-day work and family life. Here, we found a significant interaction ($F = 8.49$, $p < 0.01$) between neuron type and clinical diagnosis, such that VEN, fork cell and layer 2–3 neuron TDP-43 inclusions in right FI were more frequent among patients with behavioral symptoms sufficient to warrant a bvFTD diagnosis (ALS vs bvFTD-MND or bvFTD, $p < 0.005$) (Fig. 2e). Although patients with clinical ALS showed only rare TDP-43 inclusions in VENs (inclusion fraction 2.6%) and fork cells (inclusion fraction 2.4%), these VEN/fork cell inclusions were 3–4 times more frequent than TDP-43 inclusions in the other right FI cell types we studied (neighboring layer 5 neurons: 0.7%, layer 2–3 neurons: 0.6%). Nuclear TDP-43-depleted VENs and fork cells were more frequent in ALS than in bvFTD (Fig. 2f and Suppl. Figure 4a), suggesting that loss of nuclear TDP-43, through whatever mechanism, may precede TDP-43 aggregation. To assess whether selective VEN/fork pathobiology can be detected even in patients with pure ALS, we combined TDP-43 depletion and aggregation measures in this group and compared this composite measure across cells types (Suppl. Figure 4a., S1–S4). The results show that 11.4% (left) and 11.5% (right) of VENs and 11.0% (left) and 8.9% (right) of fork cells show TDP-43 pathobiology in pure ALS, represnting a four to fivefold increase over neighboring layer 5 neurons (VENs: $t = 9.75$, $p < 0.0001$; fork cells: $t = 10.67$, $p < 0.0001$) and a two to threefold increase over layer 2–3 neurons (VENs: $t = 2.59$, $p = 0.30$; fork cells: $t = 3.49$, $p = 0.034$).

In contrast to a previous study of later stage bvFTD, in which greater functional impairment (CDR sum of boxes) correlated with right hemisphere VEN and fork cell

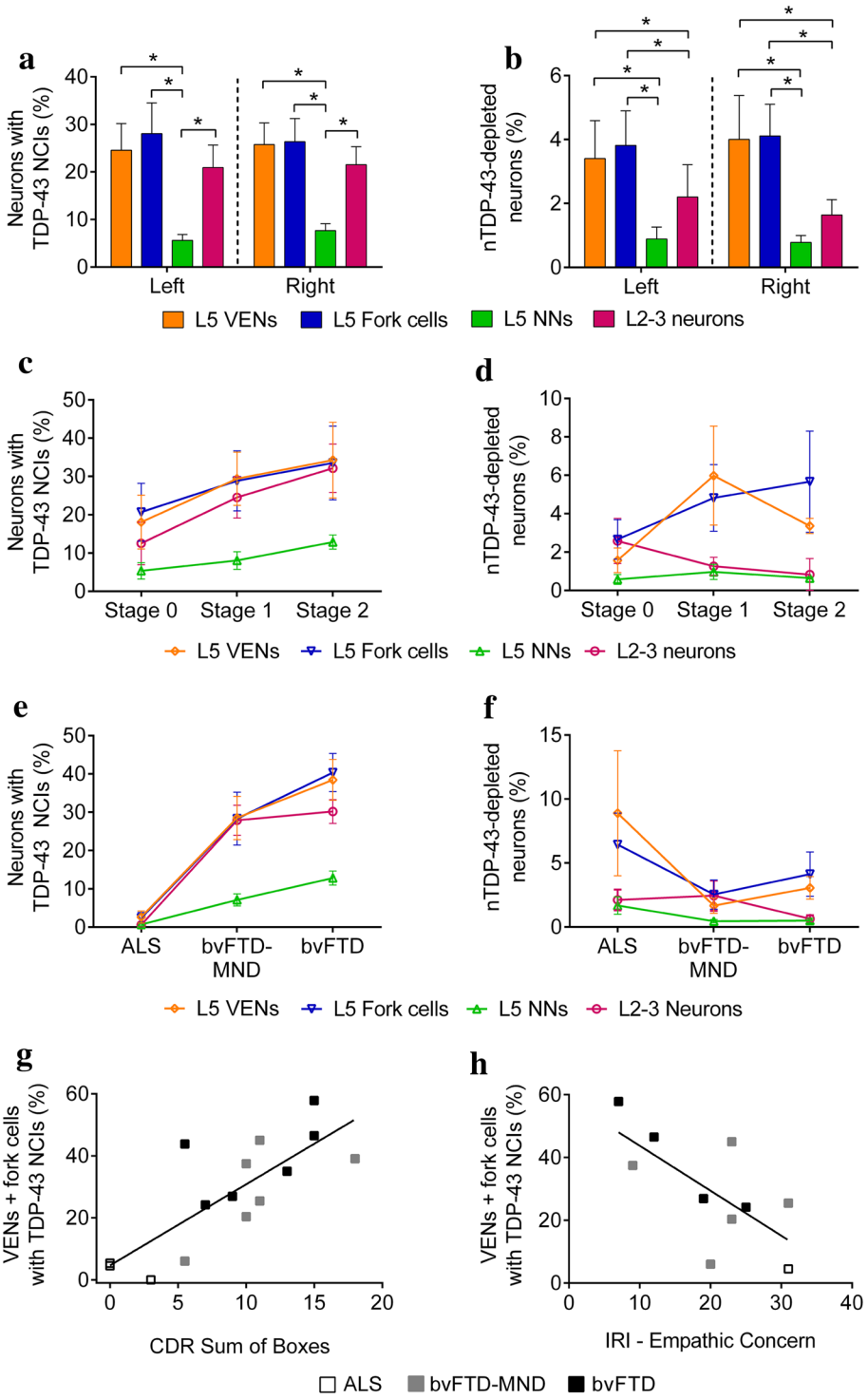

Fig. 2 FI layer 5 VENs, fork cells and layer 2–3 neurons show increased propensity for TDP-43 inclusions in sporadic bvFTD/MND. **a** Layer 5 (L5) VENs and fork cells, and layer 2–3 (L2–3) neurons were significantly more prone to TDP-43 neuronal cytoplasmic inclusions (NCIs) than were neighboring layer 5 non-VEN/fork neurons (L5 NNs). **b** L5 VENs and fork cells showed significantly more nuclear TDP-43-depletion than L5 NNs or L2-3 neurons. *$p<0.01$. The patterns of TDP-43 inclusion formation and nuclear TDP-43 depletion were similar in left and right FI (**a**, **b**). **c** VEN and fork cell TDP-43 aggregation emerged in the absence of gross atrophy (Broe stage 0), while L5 NNs showed low inclusion fractions. TDP-43 inclusion formation rates in layer 2–3 neurons appeared to more closely follow VENs and fork cells. **d** At Broe stages 0–2, depletion of nuclear TDP-43, without formation of overt cytoplasmic inclusions, (nTDP-43 depletion) was observed in a small percentage of VENs, fork cells, and layer 2–3 neurons. **e** VEN, fork cell, and L2–3 neuron inclusions were infrequent in ALS but were present by behavioral symptom onset ($p<0.005$). **f** In contrast, nuclear TDP-43 depletion without NCI formation was more prominent in VENs and fork cells than layer 2–3 neurons and layer 5 neighboring neurons in ALS cases. Data in **b**–**e** are shown as group mean ± SEM from right FI. Data for Stage 2 in **c**, **d** are shown as mean and range ($n=2$ Broe stage 2 subjects with right FI). **g**, **h** The proportion of VENs and fork cells with TDP-43 inclusions correlated with Clinical Dementia Rating (CDR) (**g**) and inversely correlated with empathic concern (**h**) in the right hemisphere. For clarity, only VENs + fork cells (combined) are shown in **g** and **h**

dropout [34], in the present study, it was the proportion of right hemisphere TDP-43 inclusion-bearing neurons that predicted greater impairment (VENs + fork cells: $r=0.83$, $p=0.00048$, Fig. 2g; neighboring layer 5 neurons: $r=0.82$, $p=0.00062$; layer 2–3 neurons: $r=0.63$, $p=0.025$). Using a more specific measure of social–emotional dysfunction, the Interpersonal Reactivity Index (IRI), we found that the fraction of right hemisphere layer 5 neurons bearing TDP-43 inclusions predicted deficits in emotional empathy (IRI, empathic concern subscale; VENs + fork cells: $r=-0.69$, Fig. 2h), $p=0.038$; neighboring layer 5 neurons: $r=-0.69$, $p=0.039$). Layer 2–3 neuron inclusion fractions did not correlate with measures of empathic concern ($r=-0.30$, $p=0.47$). Right FI inclusion fractions in VENs, fork cells,

and neighboring layer 5 neurons showed high multi-collinearity (spearman correlation coefficients 0.75–0.96; variance inflation factor = 3.56–5.51), precluding mediation analysis to determine which cell type was most likely driving the behavioral change. CDR (VENs: $r = 0.073$, $p = 0.81$; fork cells: $r = -0.18$, $p = 0.55$; neighboring layer 5 neurons: $r = 0.34$, $p = 0.25$) and empathic concern (VENs: $r = -0.010$, $p = 0.98$; fork cells: $r = -0.12$, $p = 0.75$; neighboring layer 5 neurons: $r = 0.023$, $p = 0.95$) showed no correlation with neuronal densities. Collectively, these findings suggest that, in early stages of bvFTD, TDP-43 inclusion formation may lead to targeted neuronal dysfunction that contributes to clinical deficits despite limited neuronal loss.

VENs and fork cells show increased TDP-43 aggregation and nuclear depletion in the *C9orf72*-bvFTD/MND spectrum

The *C9orf72* hexanucleotide repeat expansion is the major genetic cause of inherited FTD/ALS [18, 61] and is almost always accompanied by TDP-43 proteinopathy [43, 49]. In addition, *C9orf72* expansions are associated with several additional pathological features, including repeat RNA foci [18] and dipeptide repeat protein inclusions [4, 48]. Therefore, for this study, we elected to separate the *C9orf72* and sporadic patients in our cohort. We retained and randomized ten patients with *C9orf72*-bvFTD/MND to neuron quantification runs so that raters would remain blind to genetic status, enabling a future blinded study comparing sporadic to *C9orf72*-bvFTD/MND. An interim analysis of TDP-43 inclusions in VENs, fork cells, and neighboring layer 5 neurons in the *C9orf72* group, however, provided data critical to the understanding of our sporadic bvFTD/MND findings, so we elected to present this analysis here. We observed no significant neuronal loss in patients with *C9orf72* FTD/MND, although there was a trend toward VEN and fork cell loss (Suppl. Figure 3f) that mirrored the degree of neuronal loss observed in the sporadic FTD/MND group (Suppl. Figure 3a). Although the overall proportion of neurons forming TDP-43 inclusions was much lower in *C9orf72*-bvFTD than in sporadic bvFTD, VENs ($t = 3.82$, $p = 0.00013$) and forks cells ($t = 4.36$, $p < 0.0001$) were again four times more vulnerable to TDP-43 inclusions than were neighboring layer 5 neurons (Fig. 3b). Interestingly, in *C9orf72*-bvFTD/MND, neurons lacking nuclear TDP-43 without a TDP-43 inclusion (nuclear TDP-43 depleted) were as common as neurons with TDP-43 inclusions overall (Fig. 3a, b), although these rates varied between subjects (Fig. 3c). In one *C9orf72*-ALS patient, over 20% of VENs showed nuclear TDP-43 depletion while fewer than 5% showed TDP-43 aggregation (Fig. 3c).

VENs and fork cells with nuclear TDP-43 depletion, with or without aggregation, show nuclear and somatodendritic atrophy

Having shown that VENs and fork cells are more prone to TDP-43 aggregation and nuclear depletion, we next asked how these specific phenomena relate to the morphological integrity of individual neurons. To our knowledge, no human study has quantified the relationship between TDP-43 pathobiology and neuronal morphology, perhaps because the enormous variation in cortical neuron size and shape would undermine implementation of such efforts. VENs and fork cells, being relatively homogeneous, provided an opportunity to overcome these issues. Indeed, upon visual inspection, VENs and fork cells with TDP-43 inclusions or depletion exhibited a shrunken, degenerate morphology (Fig. 1 and Suppl. Figure 5a). We further noted that, in patient tissues, inclusion-lacking VENs and fork cells with normal nuclear TDP-43 were often unusually large. Consistent with these observations, morphometric analysis confirmed that TDP-43 aggregation is associated with atrophy across multiple measures (Fig. 4a, b). VEN somatic ($t = -13.37$, $p < 0.00001$) and nuclear area ($t = -10.90$, $p < 0.00001$) and apical ($t = -18.91$, $p < 0.00001$) and basal ($t = -17.48$, $p = 0.00001$) dendritic diameters were smaller in cells with cytoplasmic TDP-43 aggregation than unaffected neurons (Fig. 4a). The pattern in fork cells (Fig. 4b) mirrored that seen in VENs: somatic ($t = -6.33$, $p < 0.00001$) and nuclear area ($t = -7.16$, $p < 0.00001$) and apical ($t = -15.90$, $p < 0.00001$) and basal ($t = -11.92$, $p < 0.00001$) dendritic diameters were smaller in fork cells with cytoplasmic TDP-43 inclusions than fork cells with normal nuclear TDP-43. Inclusion-bearing pyramidal neurons showed reduced apical ($t = -5.86$, $p = 4.64 \times 10^{-9}$) and basal dendritic diameter ($t = -2.10$, $p = 0.036$), but no change in nuclear ($t = 0.63$, $p = 0.52$) or somatic ($t = 1.15$, $p = 0.24$) area (Suppl. Figure 5b). The findings were not influenced by *C9orf72* status overall (genotype as a fixed effect was not significant).

TDP-43 inclusion formation is universally accompanied by a loss of nuclear TDP-43. In the course of the present work, our recognition of the nuclear TDP-43-depleted neurons indicated that the reverse is not necessarily true (Fig. 1c and Suppl. Figure 4a). This dissociation suggested an avenue for informing the ongoing controversy about whether neuronal degeneration in TDP-43 proteinopathy results from inclusion toxicity or a loss of TDP-43 function. In our data, nuclear TDP-43-depleted VENs and fork cells showed somatodendritic and nuclear atrophy (Fig. 4a, b; VENs: somatic area, $t = -11.80$, $p < 0.00001$; nuclear area, $t = -10.22$, $p < 0.00001$; apical dendritic diameter, $t = -16.57$, $p < 0.00001$; basal dendritic diameter, $t = -16.01$, $p < 0.00001$; fork cells: somatic area, $t = -6.43$, $p < 0.00001$; nuclear area, $t = -6.64$,

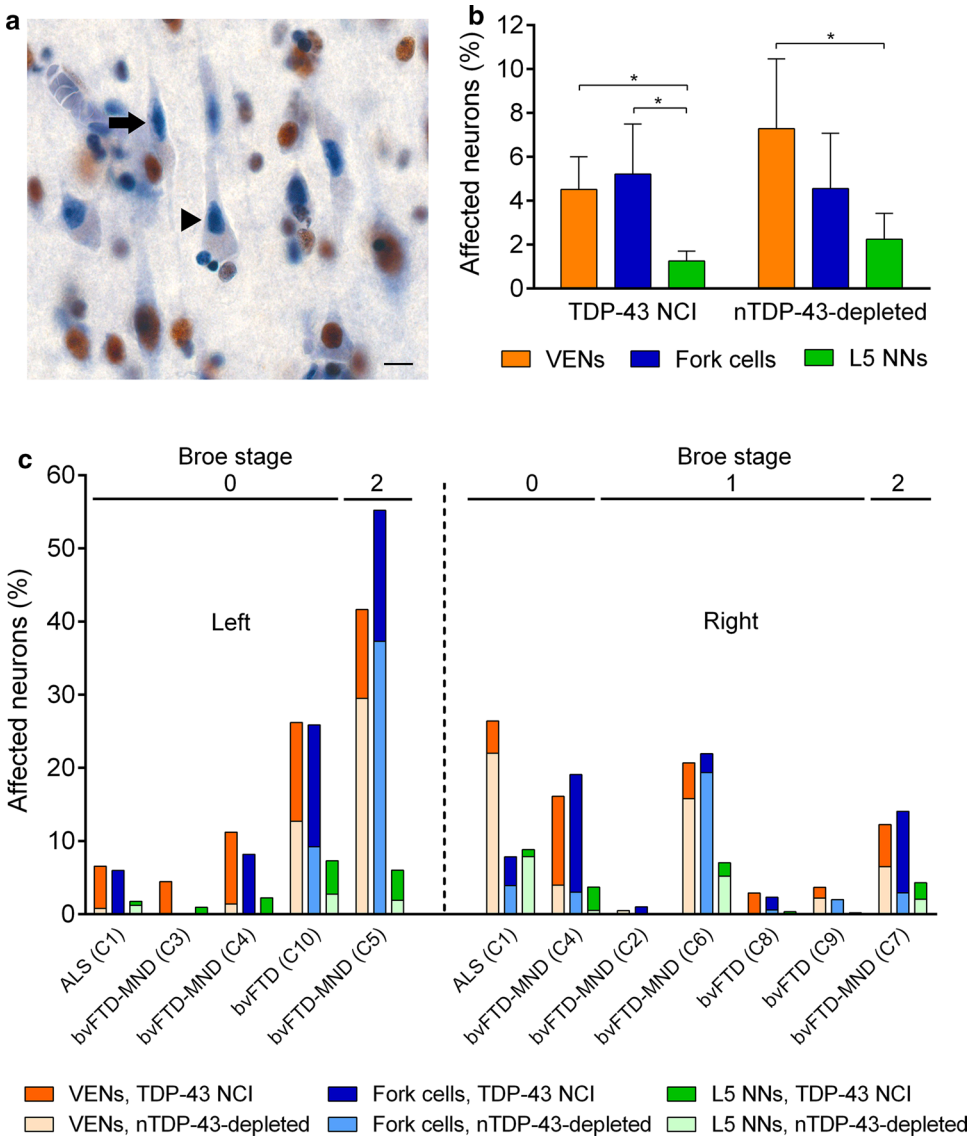

Fig. 3 VENs and fork cells are also prone to TDP-43 inclusion formation in *C9orf72*-bvFTD/MND. **a** Nuclear TDP-43-depleted neurons were more frequent in *C9orf72*-bvFTD/MND (arrow: VEN, arrowhead: pyramidal neuron). Scale bar in (**a**) represents 10 µm. **b** In *C9orf72*-bvFTD/MND, VENs and fork cells were also more prone to TDP-43 neuronal cytoplasmic inclusions (NCIs) and nuclear TDP-43 depletion without NCIs (nTDP-43 depleted) than neighboring layer 5 neurons (L5 NNs) although TDP-43 inclusion formation in VENs and fork cells occurred at a lower rate in *C9orf72*-bvFTD/MND than sporadic bvFTD/MND. Data in (**b**) is from the right hemisphere and is shown as mean ± SEM. *$p < 0.02$ compared with L5 NNs. **c** Percentage of affected (TDP-43 NCI and nuclear TDP-43-depleted) neurons in layer 5 of the FI in each patient with *C9orf72*-bvFTD/MND. The fraction of VENs, fork cells, and neighboring layer 5 neurons with TDP-43 depletion was as high as the fraction of neurons with TDP-43 inclusions in six of the *C9orf72*-bvFTD/MND cases

$p < 0.00001$; apical dendrite diameter, $t = -12.01$, $p < 0.00001$; basal dendritic diameter, $t = -9.86$, $p < 0.00001$) just as severe as that seen in inclusion-bearing neurons, suggesting that loss of nuclear TDP-43 function alone proves deleterious. We observed no significant differences between inclusion-bearing and nuclear TDP-43-depleted VENs ($t = -1.38$ to -0.61, $p = 0.17$–0.54) or fork cells ($t = -1.76$–0.33, $p = 0.079$–0.74) for any neuronal compartment. In layer 5 pyramidal neurons, somata ($t = -2.17$, $p = 0.03$) but not nuclei or dendrites ($t = -1.37$ to -0.52, $p = 0.17$–0.60), were significantly smaller in nuclear TDP-43-depleted cells than those with TDP-43 inclusions. Remarkably, for reasons that remain uncertain, VENs with normal TDP-43 localization showed larger nuclear (VENs: $t = 2.00$, $p = 0.045$) and somatic (VENs: $t = 2.28$, $p = 0.022$) areas in patients than in controls.

Our morphometric data suggested that, in patients, VENs and fork cells might each be divided into 2–3 neuronal classes or "states". To pursue this idea, we used *K*-means clustering, an iterative data partitioning algorithm that assigns a set of observations to a predefined number of clusters, to classify VENs into three clusters (Fig. 4c) based on their somatic and nuclear area but without using information about the source (patient vs. control) or TDP-43 status (inclusion-bearing, depleted, or unaffected). Although assigned to clusters without regard to TDP-43 status, VENs were unevenly distributed across clusters according to TDP-43 status (Suppl. Table 4, $\chi^2 = 135.48$, $p < 0.0001$). TDP-43 inclusion-bearing and depleted neurons clustered together (Cluster 3). Neurons with normal TDP-43 were spread over two clusters. Cluster 1 was composed of predominantly normal cells from patients, whereas Cluster 2 had normal cells from healthy controls along with some TDP-43 inclusion-bearing or nuclear-depleted neurons from patients.

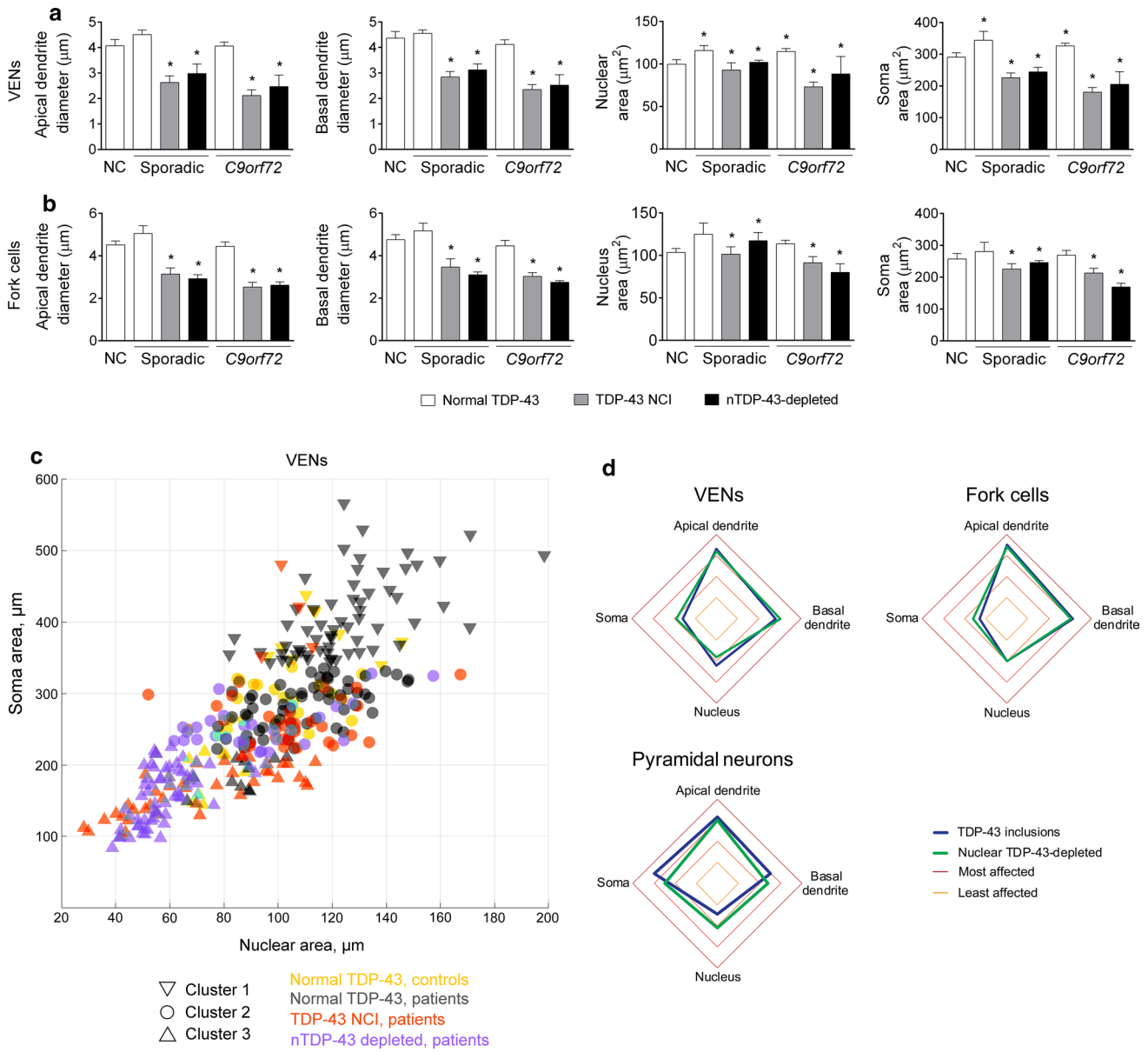

Fig. 4 TDP-43 aggregation and TDP-43 depletion are linked to VEN and fork cell atrophy in both sporadic and *C9orf72*-bvFTD/MND. **a**, **b** Morphometric analyses revealed that VEN (**a**) and fork cell (**b**) somatic and nuclear area, and apical and basal dendritic diameter were significantly smaller (20–39%) in cells with TDP-43 neuronal cytoplasmic inclusions (NCIs) than those without in bvFTD/MND patients. Somatodendritic atrophy was also evident in nuclear TDP-43-depleted neurons without NCIs (nTDP-43-depleted). Intriguingly, VENs (**a**) with normal nuclear TDP-43 in bvFTD patients showed higher nuclear (16%) and somatic area (18%) compared to VENs in controls. Normal VENs and fork cells neurons in bvFTD had a significantly larger nucleus and soma than TDP-43 inclusion-bearing and nuclear TDP-43-depleted neurons. Data in **a** and **b** are shown as mean ± SEM, with the mean and range shown for nuclear TDP-43-depleted neurons in sporadic cases (nuclear TDP-43-depleted VENs and fork cells were identified in two of the sporadic cases that underwent morphometric analysis). $*p < 0.05$ compared with normal controls. **c** Clustering analysis of VEN nucleus and soma area, and apical and basal dendritic diameter identified three clusters, primarily corresponding to normal cells from patients (cluster 1) and inclusion-bearing/nuclear TDP-43-depleted VENs (cluster 3), with normal cells from control subjects and some TDP-43 inclusion/depleted neurons combined in cluster 2. Only two (nuclear and soma area) of the four parameters used to define clusters are shown for clarity. **d** Apical dendrites, followed by basal dendrites, were the most affected compartments in TDP-43 inclusion-bearing and nuclear TDP-43-depleted VENs and fork cells, with the highest mean rank, corresponding to highest z score

Overall, these findings further support the view that neurons with TDP-43 inclusions or nuclear depletion are characterized by similar atrophy profiles, while normal neurons from patients are larger than normal neurons in controls.

To further characterize how TDP-43 pathobiological states influenced the pattern of atrophy across the four neuronal compartments (i.e., soma, nucleus, apical dendrite, and basal dendrite; Fig. 4d and Suppl. Tables 5 and 6), we ranked each TDP-43 inclusion-bearing or TDP-43 nuclear-depleted neuron in terms of which compartment was most to least affected compared to control neurons of the same type. Across the three neuron types and two TDP-43 pathobiological states, we found a relationship between atrophy severity rankings and neuronal compartment (Suppl. Table 5). In TDP-43 inclusion-bearing and nuclear TDP-43-depleted VENs and fork cells, the apical dendrite was most affected, followed by the basal dendrite, nucleus, then soma (Fig. 4d and Suppl. Table 6). The apical dendrite was most affected in pyramidal neurons with TDP-43 inclusions, while apical and soma were the two most affected compartments in pyramidal neurons with nuclear TDP-43 depletion (Fig. 4d and Suppl. Table 6).

Discussion

In many neurodegenerative disorders, early neuronal loss targets a specialized pool of regionally concentrated and morphologically unique neurons [28, 31]. In bvFTD, this pool is composed of the VENs and fork cells of the anterior cingulate and frontoinsular cortices. Here, we leveraged this anatomical framework to provide new insights into selective vulnerability and TDP-43 pathobiology. Our study identifies VENs and fork cells as an early target of TDP-43 pathobiology in bvFTD and shows that VEN and fork cell TDP-43 aggregation (1) correlates with regional atrophy and behavioral symptoms, (2) occurs in both sporadic and *C9orf72* bvFTD/MND, and (3) is linked to nuclear and somatodendritic atrophy at the level of individual neurons. In addition, we show that loss of nuclear TDP-43 can occur in the absence of, or perhaps prior to, overt TDP-43 aggregation and may be sufficient to induce neurodegeneration. These novel human findings have major implications for the pathogenesis and future treatment of FTD, ALS, and other disorders associated with TDP-43 inclusion pathology, suggesting that loss of nuclear TDP-43 function may be the earliest and most consequential aspect of TDP-43 pathobiology. At the very least, the findings show that mature TDP-43 inclusions, though they may be deleterious, are not required for neuronal degeneration in FTD/MND.

VENs and fork cells are selectively prone to TDP-43 aggregation at the earliest stages of sporadic bvFTD

Several studies have demonstrated ACC VEN loss as a general feature of the bvFTD syndrome, including patients with underlying FTLD-TDP, -tau or -FUS [63–65, 86]. Only one previous study examined FI [34], also across the FTLD spectrum, and found 53% VEN and 68% fork cell loss in bvFTD and bvFTD-MND. No previous study has assessed VEN or fork cell disease protein aggregation in bvFTD. In the previous study of FI, VEN and fork cell dropout was greatest in patients with FTLD-tau, FTLD-FUS, and FTLD-TDP without MND [24], likely because MND often truncates the disease course when it accompanies bvFTD. We therefore focused the present study on TDP-43, the most common bvFTD-related disease protein, and on patients representing points along the bvFTD-MND spectrum, hoping to capture stages prior to severe VEN dropout during which the anatomical correlates of bvFTD symptoms are just beginning to emerge. Due to these efforts, the present sample showed only a 32% reduction in FI VEN density and a 24% reduction in fork cell density, making this the mildest bvFTD sample studied to date and allowing us to probe TDP-43 pathobiology in surviving neurons. We included patients with ALS because we hypothesized that, just as some patients with pure bvFTD show TDP-43 aggregation in scattered motor neurons, some patients with pure ALS might show TDP-43 inclusions in VENs and fork cells. Confirming our hypothesis, and in line with a qualitative study identifying VEN TDP-43 depletion in pure ALS [6], we found that the proportion of VENs and fork cells with TDP-43 inclusions in pure ALS was low but higher than seen in the other cell types we studied. Separating patients by clinical diagnosis and atrophy severity suggested that VENs and fork cells are affected during the earliest identifiable stages, at a time when layer 2–3 neurons are just beginning to form TDP-43 inclusions and when neighboring layer 5 neurons are still largely spared. In patients with more advanced clinical–anatomical deficits, layer 2–3 neurons become nearly as affected as VENs and fork cells, whereas inclusions in layer 5 non-VEN/fork neurons rise only slightly. Nonetheless, the strong link between TDP-43 aggregation and clinical measures suggests that TDP-43 pathobiology is sufficient to induce neuronal dysfunction, leading to behavioral deficits, even while neuronal loss remains mild or absent. The characteristic "speckled" dot- and dash-like TDP-43 inclusions in VENs and fork cells have been described by some as early stage "pre-inclusions", which often show only partial ubiquitination, as observed here (Fig. 1d) [25, 29, 71].

VEN and fork cell involvement in *C9orf72*-bvFTD/MND

As in sporadic bvFTD/MND, [6] in *C9orf72*-bvFTD/MND VENs and fork cells were more prone to TDP-43 inclusion formation compared to neighboring layer 5 neurons. Interestingly, although overall rates of TDP-43 inclusion formation were lower in *C9orf72*-bvFTD/MND, VEN and fork

cell density reductions were nearly identical to those seen here in sporadic bvFTD/MND and consistent with a previous *C9orf72*-bvFTD study of VEN dropout in the anterior cingulate cortex [86]. The low TDP-43 inclusion fractions might suggest that *C9orf72*-specific disease mechanisms, such as repeat RNA foci and dipeptide repeat protein inclusions [4, 61], contribute to neuronal dysfunction and death in *C9orf72*-bvFTD and ALS or that other brain regions contribute to bvFTD-related network dysfunction [37, 86]. Alternatively, *C9orf72*-specific pathological features may sensitize vulnerable neurons to TDP-43 pathobiology, such that early stage TDP-43 mislocalization and aggregation lead to accelerated neuronal dropout. Although some human *C9orf72*-FTD/MND studies have suggested a strong correlation between regional TDP-43 aggregation and neurodegeneration [43], our previous work has shown that TDP-43 aggregation can be scarce or even absent in patients with clinical *C9orf72*-bvFTD [78]. Future studies should examine the frequency of other *C9orf72*-specific pathological phenomena in VENs and fork cells and the relationship of these features to TDP-43 nuclear depletion and cytoplasmic aggregation.

Our data, however, suggest a third possibility: that VEN and fork cell dysfunction in *C9orf72*-bvFTD/MND may relate to depletion of nuclear TDP-43 without, or prior to, inclusion formation. This "nuclear TDP-43-depleted" state was also seen, albeit less often, in the sporadic patients, where nuclear TDP-43 depletion without NCI formation was particularly prominent in pure ALS. Only three previous studies have reported nuclear TDP-43-depleted neurons in ALS or FTD [6, 7, 78]. Depletion of nuclear TDP-43 may represent a separate pathway toward neurodegeneration, perhaps related to nuclear import/export dysfunction [58], or a transitional state en route to TDP-43 aggregation. A previous report from our group characterized temporal lobe resection (for epilepsy) and autopsy tissue from the same *C9orf72*-FTD patient and found nuclear TDP-43 depletion without aggregation in the resection specimen taken 5 years prior to symptom onset but prominent TDP-43 inclusion pathology at autopsy 13 years later [78]. These finding, together with the present study, suggest the possibility that nuclear TDP-43 depletion may ultimately transition toward aggregate formation within the same neurons.

Association of TDP-43 aggregation and nuclear depletion with neuronal atrophy

Microscopic examination of patient tissue suggested striking size differences between inclusion-bearing neurons and inclusion-lacking neurons with normal nuclear TDP-43, leading us to undertake a detailed morphometric study. In sporadic and *C9orf72*-bvFTD/MND, VEN and fork cell apical and basal dendritic diameter and nuclear and somatic area were significantly shrunken in neurons with TDP-43 inclusions compared to those without. Many studies in model systems suggest that TDP-43 overexpression and aggregation lead to cell dysfunction and death [5, 77, 84, 85], but no previous human neuropathologic study has linked TDP-43 pathobiology to degeneration at the level of individual neurons. Moreover, it has remained unclear whether TDP-43 aggregate toxicity or loss of normal nuclear TDP-43 function is the key driver of pathogenesis in patients. Our data show that nuclear TDP-43-depleted neurons develop somatodendritic and nuclear atrophy similar to that seen in inclusion-bearing neurons. This crucial observation suggests that loss of nuclear TDP-43 function may be sufficient to undermine neuronal integrity in vivo. Our data also suggest that TDP-43 aggregation—at least the type visible using conventional methods—may not be necessary for neurodegeneration. Despite the lack of a visible TDP-43 NCI in these nuclear TDP-43-depleted neurons, it is possible that low levels of a toxic non-aggregated form of cytoplasmic TDP-43, below the detection threshold of our staining protocol, are contributing to the morphometric deficits seen in these neurons, in keeping with model system findings in which elevated but non-aggregated cytoplasmic TDP-43 precipitates cell death [5]. In addition, it is possible that undetected low levels of nuclear TDP-43 remain in these neurons and are sufficient to support normal TDP-43 function. Despite these caveats, our data suggest that loss of nuclear TDP-43 function deserves major consideration as a contributor to pathogenesis in FTLD-TDP and ALS-TDP.

In sporadic ALS, upper motor neurons and VENs have also been reported to show clearing of nuclear TDP-43 without cytoplasmic TDP-43 aggregation [6, 7]. Identification of the nuclear TDP-43-depleted VENs and fork cells provides an opportunity for future studies to explore neurodegeneration mechanisms associated with TDP-43 loss-of-function. Interestingly, conditional mouse models overexpressing a human form of TDP-43 with a mutated nuclear localization signal develop behavioral and motor changes with little TDP-43 aggregation [1, 32], relating to suppression of mouse TDP-43 expression. Likewise, mice expressing a common human mutation in TDP-43 showed no TDP-43 aggregation but frequent nuclear TDP-43 depletion, accompanied by progressive neuromuscular weakness and death [83]. Recently, novel hypotheses have emerged about how loss of nuclear TDP-43 function may lead to neuronal dysfunction and degeneration. In mouse embryonic stem cell, HeLa cell, and conditional TDP-43 knockout mouse models, TDP-43 mutations, depletion, or sequestration into inclusions lead to aberrant splicing [3, 38, 56, 75] and altered expression of numerous proteins [57, 70], including those involved in nucleocytoplasmic transport, RNA processing, and DNA repair. Loss of nuclear TDP-43 results in, for example, incorporation of cryptic exons into mRNAs [33, 38, 74, 75]; often such exons introduce frameshifts or

premature stop codons that lead the transcript to undergo nonsense-mediated decay. The selective vulnerability framework and experimental platform developed through this study can now be used to explore these potential mechanisms directly in human tissues.

VENs and fork cells with normal nuclear TDP-43 were larger in patients with bvFTD than in control subjects and much larger than the atrophied inclusion-bearing and nuclear TDP-43-depleted neurons seen within the same patients. This unexpected observation could reflect compensation for other degenerating neurons in the circuit or a stage of disease just prior to nuclear TDP-43 depletion and aggregation. Strikingly, TDP-43 targets another population of large, long-range projection neurons—the upper motor neurons lost in ALS [2, 52]. We hypothesize that there are common features among VENs, fork cells, and upper motor neurons that render them particularly vulnerable to TDP-43-related degeneration. Like corticospinal motor neurons, VENs and fork cells are large layer 5 projection neurons with likely subcerebral targets [15]. In a mutant SOD1 mouse model of ALS, vulnerable populations of spinal motor neurons showed an initial increase in soma cross-sectional area, followed by atrophy later in disease [21]. This alteration in cell size was predicted to result in altered neuronal excitability [21]. Hyperexcitability is an established early feature of ALS, seen across humans [22, 80], mouse models [55] and induced pluripotent stem cell-derived neurons studies [19, 81], including motor neurons from patients with *C9orf72*-ALS [19]. Cortical hyperexcitability is described in early stage sporadic [80] and *C9orf72*-associated ALS [26]. In VENs and fork cells, similar hyperexcitability mechanisms could increase neuronal size before giving way to TDP-43 pathobiology and neuronal atrophy as neurons progress toward death.

VENs and fork cells appear to be more prone to nuclear TDP-43 depletion and aggregation (present data) but also more vulnerable to death [34, 65] in the face of TDP-43 pathobiology. It will be important to determine whether the increased rates of VEN and fork cell death result only from their increased proneness to TDP-43 pathobiology or whether they are also more likely than other cells to die once TDP-43 pathobiology emerges. Post-mortem studies cannot trace a neuron's course from nuclear TDP-43 depletion to aggregation to degeneration to ultimate cell dropout, and commonly used laboratory mammals lack VENs and fork cells. For these reasons, a natural next step in pursuing this work would be to develop human cell-based in vitro assays, akin to human iPSC-derived motor neuron assays used in ALS research. Such an approach would enable observation of longitudinal VEN/fork cell trajectories and experimental manipulations that can determine causal influence. On the other hand, still much more can be done with human tissue, following the model provided here, to determine which cellular events associated with TDP-43 pathobiology are most strongly linked to neuronal degeneration.

The impact of VEN and fork cell degeneration on large-scale network function has yet to be elucidated. The ACC and FI, key regions affected early in bvFTD [66, 87, 88], are involved in social and emotional function [16, 73]. The FI plays an important role in autonomic function, representing the internal milieu [16, 50], and connects with limbic and autonomic brain regions, including ACC, amygdala, ventral striatum, and brainstem. Intriguingly, the present study links VEN and fork cell inclusion formation with deficits in empathic concern for others. Although we have previously shown that VEN and fork cell loss correlates with behavioral symptom severity in bvFTD [34], the present study is the first to correlate inclusion formation in VENs and fork cells, or any other neuron population, with a specific social–emotional deficit. Most likely, the relationship between these cell types and emotional empathy is not one-to-one but mediated by the large-scale networks anchored by these and other FI neurons. Future studies could investigate links between the cellular, network, and behavioral levels. VENs and fork cells are thought to have subcerebral projections [15], although their precise connections are still under study in the macaque [23]. VENs and fork cells express the alpha 1a adrenergic receptor (ADRA1A), the GABA-A receptor theta subunit (GABRQ), and the vesicular monoamine transporter (VMAT2), suggesting a role for VENs and fork cells in autonomic control circuits [20]. Thus, autonomic dysfunction in bvFTD, which we have strongly linked to ACC and FI degeneration and dysfunction [30, 72], may be initiated by FI VEN and fork cell dysfunction and degeneration before spreading throughout the system to undermine some of our most specialized social–emotional capacities.

Acknowledgements This study was supported by NIH grants R01AG033017 (WWS), P01AG019724 and P50AG023501 (BLM), and the John Douglas French Alzheimer's Foundation (GC). LL was supported by the Reserve Talents of Universities Overseas Research Program of Heilongjiang in China (Document Number: Heijiaogao [2012]381). We thank the patients and their families for their invaluable contributions to FTD/MND research.

Author contributions ALN, MS, JLH, SEG, LL, EJK, and YP performed the experiments and cell counting. MS performed morphometric analysis. ALN, LP, and IEA analyzed the data. WWS, LTG, and EJH performed neuropathological diagnoses. DHG and GHC performed genetic analysis. JHK, BLM, and WWS obtained behavioral and clinical data. WWS, SEG, and ALN conceived and designed the project. WWS, and ALN wrote the paper. All authors reviewed the manuscript.

Compliance with ethical standards

Conflict of interest The authors declare that they have no conflict of interest.

References

1. Alfieri JA, Pino NS, Igaz LM (2014) Reversible behavioral phenotypes in a conditional mouse model of TDP-43 proteinopathies. J Neurosci 34:15244–15259. https://doi.org/10.1523/jneurosci.1918-14.2014
2. Arai T, Hasegawa M, Akiyama H, Ikeda K, Nonaka T, Mori H et al (2006) TDP-43 is a component of ubiquitin-positive tau-negative inclusions in frontotemporal lobar degeneration and amyotrophic lateral sclerosis. Biochem Biophys Res Commun 351:602–611. https://doi.org/10.1016/j.bbrc.2006.10.093
3. Arnold ES, Ling SC, Huelga SC, Lagier-Tourenne C, Polymenidou M, Ditsworth D et al (2013) ALS-linked TDP-43 mutations produce aberrant RNA splicing and adult-onset motor neuron disease without aggregation or loss of nuclear TDP-43. Proc Natl Acad Sci USA 110:E736–E745. https://doi.org/10.1073/pnas.1222809110
4. Ash PE, Bieniek KF, Gendron TF, Caulfield T, Lin WL, Dejesus-Hernandez M et al (2013) Unconventional translation of C9ORF72 GGGGCC expansion generates insoluble polypeptides specific to c9FTD/ALS. Neuron 77:639–646. https://doi.org/10.1016/j.neuron.2013.02.004
5. Barmada SJ, Skibinski G, Korb E, Rao EJ, Wu JY, Finkbeiner S (2010) Cytoplasmic mislocalization of TDP-43 is toxic to neurons and enhanced by a mutation associated with familial amyotrophic lateral sclerosis. J Neurosci 30:639–649. https://doi.org/10.1523/jneurosci.4988-09.2010
6. Braak H, Del Tredici K (2018) Anterior cingulate cortex TDP-43 pathology in sporadic amyotrophic lateral sclerosis. J Neuropathol Exp Neurol 77:74–83. https://doi.org/10.1093/jnen/nlx104
7. Braak H, Ludolph AC, Neumann M, Ravits J, Del Tredici K (2017) Pathological TDP-43 changes in Betz cells differ from those in bulbar and spinal α-motoneurons in sporadic amyotrophic lateral sclerosis. Acta Neuropathol 133:79–90. https://doi.org/10.1007/s00401-016-1633-2
8. Broe M, Hodges JR, Schofield E, Shepherd CE, Kril JJ, Halliday GM (2003) Staging disease severity in pathologically confirmed cases of frontotemporal dementia. Neurology 60:1005–1011
9. Brooks BR (1994) El Escorial World Federation of Neurology criteria for the diagnosis of amyotrophic lateral sclerosis. Subcommittee on Motor Neuron Diseases/Amyotrophic Lateral Sclerosis of the World Federation of Neurology Research Group on Neuromuscular Diseases and the El Escorial "Clinical limits of amyotrophic lateral sclerosis" workshop contributors. J Neurol Sci 124(Suppl):96–107
10. Brooks BR, Miller RG, Swash M, Munsat TL, World Federation of Neurology Research Group on Motor Neuron D (2000) El Escorial revisited: revised criteria for the diagnosis of amyotrophic lateral sclerosis. Amyotroph Lateral Scler Other Motor Neuron Disord 1:293–299
11. Brun A (1993) Frontal lobe degeneration of non-Alzheimer type revisited. Dementia 4:126–131
12. Brun A (1987) Frontal lobe degeneration of non-Alzheimer type. I. Neuropathology. Arch Gerontol Geriatr 6:193–208
13. Buratti E, Dork T, Zuccato E, Pagani F, Romano M, Baralle FE (2001) Nuclear factor TDP-43 and SR proteins promote in vitro and in vivo CFTR exon 9 skipping. EMBO J 20:1774–1784. https://doi.org/10.1093/emboj/20.7.1774
14. Cairns NJ, Neumann M, Bigio EH, Holm IE, Troost D, Hatanpaa KJ et al (2007) TDP-43 in familial and sporadic frontotemporal lobar degeneration with ubiquitin inclusions. Am J Pathol 171:227–240. https://doi.org/10.2353/ajpath.2007.070182
15. Cobos I, Seeley WW (2015) Human von Economo neurons express transcription factors associated with Layer V subcerebral projection neurons. Cereb Cortex 25:213–220. https://doi.org/10.1093/cercor/bht219
16. Craig AD (2009) How do you feel–now? The anterior insula and human awareness. Nat Rev Neurosci 10:59–70. https://doi.org/10.1038/nrn2555
17. Davis MH (1983) Measuring individual differences in empathy: evidence for a multidimensional approach. J Pers Soc Psychol 44:113–126
18. DeJesus-Hernandez M, Mackenzie I, Boeve B, Boxer A, Baker M, Rutherford N et al (2011) Expanded GGGGCC hexanucleotide repeat in noncoding region of C9ORF72 causes chromosome 9p-linked FTD and ALS. Neuron 72:245–256. https://doi.org/10.1016/j.neuron.2011.09.011
19. Devlin AC, Burr K, Borooah S, Foster JD, Cleary EM, Geti I et al (2015) Human iPSC-derived motoneurons harbouring TARDBP or C9ORF72 ALS mutations are dysfunctional despite maintaining viability. Nat Commun 6:5999. https://doi.org/10.1038/ncomms6999
20. Dijkstra AA, Lin LC, Nana AL, Gaus SE, Seeley WW (2018) Von Economo neurons and fork cells: a neurochemical signature linked to monoaminergic function. Cereb Cortex 28:131–144. https://doi.org/10.1093/cercor/bhw358
21. Dukkipati SS, Garrett TL, Elbasiouny SM (2018) The vulnerability of spinal motoneurons and soma size plasticity in a mouse model of amyotrophic lateral sclerosis. J Physiol. https://doi.org/10.1113/jp275498
22. Eisen A, Pant B, Stewart H (1993) Cortical excitability in amyotrophic lateral sclerosis: a clue to pathogenesis. Can J Neurol Sci 20:11–16
23. Evrard HC, Forro T, Logothetis NK (2012) Von Economo neurons in the anterior insula of the macaque monkey. Neuron 74:482–489. https://doi.org/10.1016/j.neuron.2012.03.003
24. Forman M, Mackenzie I, Cairns N, Swanson E, Boyer P, Drachman D et al (2006) Novel ubiquitin neuropathology in frontotemporal dementia with valosin-containing protein gene mutations. J Neuropathol Exp Neurol 65:571–581. https://doi.org/10.1097/00005072-200606000-00005
25. Fujita Y, Mizuno Y, Takatama M, Okamoto K (2008) Anterior horn cells with abnormal TDP-43 immunoreactivities show fragmentation of the Golgi apparatus in ALS. J Neurol Sci 269:30–34. https://doi.org/10.1016/j.jns.2007.12.016
26. Geevasinga N, Menon P, Nicholson GA, Ng K, Howells J, Kril JJ et al (2015) Cortical function in asymptomatic carriers and patients with C9orf72 amyotrophic lateral sclerosis. JAMA Neurol 72:1268–1274. https://doi.org/10.1001/jamaneurol.2015.1872
27. Geser F, Lee VMY, Trojanowski JQ (2010) Amyotrophic lateral sclerosis and frontotemporal lobar degeneration: a spectrum of TDP-43 proteinopathies. Neuropathology 30:103–112. https://doi.org/10.1111/j.1440-1789.2009.01091.x
28. Gibb WR, Lees AJ (1991) Anatomy, pigmentation, ventral and dorsal subpopulations of the substantia nigra, and differential cell death in Parkinson's disease. J Neurol Neurosurg Psychiatry 54:388–396
29. Giordana MT, Piccinini M, Grifoni S, De Marco G, Vercellino M, Magistrello M et al (2010) TDP-43 redistribution is an early event in sporadic amyotrophic lateral sclerosis. Brain Pathol 20:351–360. https://doi.org/10.1111/j.1750-3639.2009.00284.x
30. Guo CC, Sturm VE, Zhou J, Gennatas ED, Trujillo AJ, Hua AY et al (2016) Dominant hemisphere lateralization of cortical parasympathetic control as revealed by frontotemporal dementia. Proc Natl Acad Sci USA 113:E2430–E2439. https://doi.org/10.1073/pnas.1509184113
31. Hyman BT, Van Hoesen GW, Damasio AR, Barnes CL (1984) Alzheimer's disease: cell-specific pathology isolates the hippocampal formation. Science 225:1168–1170

32. Igaz LM, Kwong LK, Lee EB, Chen-Plotkin A, Swanson E, Unger T et al (2011) Dysregulation of the ALS-associated gene TDP-43 leads to neuronal death and degeneration in mice. J Clin Invest 121:726–738. https://doi.org/10.1172/jci44867
33. Jeong YH, Ling JP, Lin SZ, Donde AN, Braunstein KE, Majounie E et al (2017) Tdp-43 cryptic exons are highly variable between cell types. Mol Neurodegener 12:13. https://doi.org/10.1186/s13024-016-0144-x
34. Kim EJ, Sidhu M, Gaus SE, Huang EJ, Hof PR, Miller BL et al (2012) Selective frontoinsular von Economo neuron and fork cell loss in early behavioral variant frontotemporal dementia. Cereb Cortex 22:251–259
35. Knopman DS, Kramer JH, Boeve BF, Caselli RJ, Graff-Radford NR, Mendez MF et al (2008) Development of methodology for conducting clinical trials in frontotemporal lobar degeneration. Brain 131:2957–2968. https://doi.org/10.1093/brain/awn234
36. Lasch P, Haensch W, Naumann D, Diem M (2004) Imaging of colorectal adenocarcinoma using FT-IR microspectroscopy and cluster analysis. Biochim Biophys Acta Mol Basis Dis 1688:176–186. https://doi.org/10.1016/j.bbadis.2003.12.006
37. Lee SE, Sias AC, Mandelli ML, Brown JA, Brown AB, Khazenzon AM et al (2017) Network degeneration and dysfunction in presymptomatic C9ORF72 expansion carriers. Neuroimage Clin 14:286–297. https://doi.org/10.1016/j.nicl.2016.12.006
38. Ling JP, Pletnikova O, Troncoso JC, Wong PC (2015) TDP-43 repression of nonconserved cryptic exons is compromised in ALS-FTD. Science 349:650–655. https://doi.org/10.1126/science.aab0983
39. Lloyd S (1982) Least squares quantization in PCM. IEEE Trans Inf Theory 28:129–137
40. Mackenzie I, Baborie A, Pickering-Brown S, Du Plessis D, Jaros E, Perry R et al (2006) Heterogeneity of ubiquitin pathology in frontotemporal lobar degeneration: classification and relation to clinical phenotype. Acta Neuropathol 112:539–549. https://doi.org/10.1007/s00401-006-0138-9
41. Mackenzie I, Neumann M, Baborie A, Sampathu D, Du Plessis D, Jaros E et al (2011) A harmonized classification system for FTLD-TDP pathology. Acta Neuropathol 122:111–113. https://doi.org/10.1007/s00401-011-0845-8
42. Mackenzie I, Neumann M, Bigio E, Cairns N, Alafuzoff I, Kril J et al (2010) Nomenclature and nosology for neuropathologic subtypes of frontotemporal lobar degeneration: an update. Acta Neuropathol 119:1–4. https://doi.org/10.1007/s00401-009-0612-2
43. Mackenzie IR, Arzberger T, Kremmer E, Troost D, Lorenzl S, Mori K et al (2013) Dipeptide repeat protein pathology in C9ORF72 mutation cases: clinico-pathological correlations. Acta Neuropathol 126:859–879. https://doi.org/10.1007/s00401-013-1181-y
44. MacQueen J (1967) Some methods for classification and analysis of multivariate observations. In: Proceedings of the 5th Berkeley symposium on mathematical statistics and probability, University of California Press, City, pp 281-297
45. McKeith IG, Boeve BF, Dickson DW, Halliday G, Taylor JP, Weintraub D et al (2017) Diagnosis and management of dementia with Lewy bodies: fourth consensus report of the DLB consortium. Neurology 89:88–100. https://doi.org/10.1212/wnl.0000000000004058
46. McKeith IG, Dickson DW, Lowe J, Emre M, O'Brien JT, Feldman H et al (2005) Diagnosis and management of dementia with Lewy bodies: third report of the DLB consortium. Neurology 65:1863–1872. https://doi.org/10.1212/01.wnl.0000187889.17253.b1
47. Montine TJ, Phelps CH, Beach TG, Bigio EH, Cairns NJ, Dickson DW et al (2012) National Institute on Aging-Alzheimer's Association guidelines for the neuropathologic assessment of Alzheimer's disease: a practical approach. Acta Neuropathol 123:1–11. https://doi.org/10.1007/s00401-011-0910-3
48. Mori K, Weng SM, Arzberger T, May S, Rentzsch K, Kremmer E et al (2013) The C9orf72 GGGGCC repeat is translated into aggregating dipeptide-repeat proteins in FTLD/ALS. Science 339:1335–1338. https://doi.org/10.1126/science.1232927
49. Murray ME, DeJesus-Hernandez M, Rutherford NJ, Baker M, Duara R, Graff-Radford NR et al (2011) Clinical and neuropathologic heterogeneity of c9FTD/ALS associated with hexanucleotide repeat expansion in C9ORF72. Acta Neuropathol 122:673–690. https://doi.org/10.1007/s00401-011-0907-y
50. Mutschler I, Wieckhorst B, Kowalevski S, Derix J, Wentlandt J, Schulze-Bonhage A et al (2009) Functional organization of the human anterior insular cortex. Neurosci Lett 457:66–70. https://doi.org/10.1016/j.neulet.2009.03.101
51. Neary D, Snowden JS, Gustafson L, Passant U, Stuss D, Black S et al (1998) Frontotemporal lobar degeneration: a consensus on clinical diagnostic criteria. Neurology 51:1546–1554
52. Neumann M, Sampathu D, Kwong L, Truax A, Micsenyi M, Chou T et al (2006) Ubiquitinated TDP-43 in frontotemporal lobar degeneration and amyotrophic lateral sclerosis. Science 314:130–133. https://doi.org/10.1126/science.1134108
53. Ngowyang G (1932) Beschreibung einer Art von Spezialzellem in der Ins elrinde. J Psychol Neurol 44:671–674
54. Perry DC, Brown JA, Possin KL, Datta S, Trujillo A, Radke A et al (2017) Clinicopathological correlations in behavioural variant frontotemporal dementia. Brain 140:3329–3345. https://doi.org/10.1093/brain/awx254
55. Pieri M, Albo F, Gaetti C, Spalloni A, Bengtson CP et al (2003) Altered excitability of motor neurons in a transgenic mouse model of familial amyotrophic lateral sclerosis. Neurosci Lett 351:153–156
56. Polymenidou M, Lagier-Tourenne C, Hutt KR, Huelga SC, Moran J, Liang TY et al (2011) Long pre-mRNA depletion and RNA missplicing contribute to neuronal vulnerability from loss of TDP-43. Nat Neurosci 14:459–468. https://doi.org/10.1038/nn.2779
57. Prpar Mihevc S, Baralle M, Buratti E, Rogelj B (2016) TDP-43 aggregation mirrors TDP-43 knockdown, affecting the expression levels of a common set of proteins. Sci Rep 6:33996. https://doi.org/10.1038/srep33996
58. Prpar Mihevc S, Darovic S, Kovanda A, Bajc Cesnik A, Zupunski V, Rogelj B (2017) Nuclear trafficking in amyotrophic lateral sclerosis and frontotemporal lobar degeneration. Brain 140:13–26. https://doi.org/10.1093/brain/aww197
59. Rankin KP, Gorno-Tempini ML, Allison SC, Stanley CM, Glenn S, Weiner MW et al (2006) Structural anatomy of empathy in neurodegenerative disease. Brain 129:2945–2956. https://doi.org/10.1093/brain/awl254
60. Rascovsky K, Hodges JR, Knopman D, Mendez MF, Kramer JH, Neuhaus J et al (2011) Sensitivity of revised diagnostic criteria for the behavioural variant of frontotemporal dementia. Brain 134:2456–2477. https://doi.org/10.1093/brain/awr179
61. Renton A, Majounie E, Waite A, Simon-Sanchez J, Rollinson S, Gibbs J et al (2011) A hexanucleotide repeat expansion in C9ORF72 is the cause of chromosome 9p21-linked ALS-FTD. Neuron 72:257–268. https://doi.org/10.1016/j.neuron.2011.09.010
62. Sampathu D, Neumann M, Kwong L, Chou T, Micsenyi M, Truax A et al (2006) Pathological heterogeneity of frontotemporal lobar degeneration with ubiquitin-positive inclusions delineated by ubiquitin immunohistochemistry and novel monoclonal antibodies. Am J Pathol 169:1343–1352. https://doi.org/10.2353/ajpath.2006.060438
63. Santillo AF, Englund E (2014) Greater loss of von Economo neurons than loss of layer II and III neurons in behavioral variant frontotemporal dementia. Am J Neurodegener Dis 3:64–71
64. Santillo AF, Nilsson C, Englund E (2013) von Economo neurones are selectively targeted in frontotemporal dementia. Neuropathol Appl Neurobiol 39:572–579. https://doi.org/10.1111/nan.12021

65. Seeley WW, Carlin DA, Allman JM, Macedo MN, Bush C, Miller BL et al (2006) Early frontotemporal dementia targets neurons unique to apes and humans. Ann Neurol 60:660–667. https://doi.org/10.1002/ana.21055
66. Seeley WW, Crawford R, Rascovsky K, Kramer JH, Weiner M, Miller BL et al (2008) Frontal paralimbic network atrophy in very mild behavioral variant frontotemporal dementia. Arch Neurol 65:249–255. https://doi.org/10.1001/archneurol.2007.38
67. Seeley WW, Menon V, Schatzberg AF, Keller J, Glover GH, Kenna H et al (2007) Dissociable intrinsic connectivity networks for salience processing and executive control. J Neurosci 27:2349–2356. https://doi.org/10.1523/jneurosci.5587-06.2007
68. Seeley WW, Merkle FT, Gaus SE, Craig AD, Allman JM, Hof PR et al (2012) Distinctive neurons of the anterior cingulate and frontoinsular cortex: a historical perspective. Cereb Cortex 22:245–250. https://doi.org/10.1093/cercor/bhr005
69. Sollberger M, Stanley CM, Wilson SM, Gyurak A, Beckman V, Growdon M et al (2009) Neural basis of interpersonal traits in neurodegenerative diseases. Neuropsychologia 47:2812–2827. https://doi.org/10.1016/j.neuropsychologia.2009.06.006
70. Stalekar M, Yin X, Rebolj K, Darovic S, Troakes C, Mayr M et al (2015) Proteomic analyses reveal that loss of TDP-43 affects RNA processing and intracellular transport. Neuroscience 293:157–170. https://doi.org/10.1016/j.neuroscience.2015.02.046
71. Strong MJ, Volkening K, Hammond R, Yang W, Strong W, Leystra-Lantz C et al (2007) TDP43 is a human low molecular weight neurofilament (hNFL) mRNA-binding protein. Mol Cell Neurosci 35:320–327. https://doi.org/10.1016/j.mcn.2007.03.007
72. Sturm VE, Brown JA, Hua AY, Lwi SJ, Zhou J, Kurth F et al (2018) Network architecture underlying basal autonomic outflow: evidence from frontotemporal dementia. J Neurosci 38:8943–8955. https://doi.org/10.1523/JNEUROSCI.0347-18.2018
73. Sturm VE, Sollberger M, Seeley WW, Rankin KP, Ascher EA, Rosen HJ et al (2013) Role of right pregenual anterior cingulate cortex in self-conscious emotional reactivity. Soc Cogn Affect Neurosci 8:468–474. https://doi.org/10.1093/scan/nss023
74. Sun M, Bell W, LaClair KD, Ling JP, Han H, Kageyama Y et al (2017) Cryptic exon incorporation occurs in Alzheimer's brain lacking TDP-43 inclusion but exhibiting nuclear clearance of TDP-43. Acta Neuropathol 133:923–931. https://doi.org/10.1007/s00401-017-1701-2
75. Tan Q, Yalamanchili HK, Park J, De Maio A, Lu HC, Wan YW et al (2016) Extensive cryptic splicing upon loss of RBM17 and TDP43 in neurodegeneration models. Hum Mol Genet 25:5083–5093. https://doi.org/10.1093/hmg/ddw337
76. Tartaglia MC, Sidhu M, Laluz V, Racine C, Rabinovici GD, Creighton K et al (2010) Sporadic corticobasal syndrome due to FTLD-TDP. Acta Neuropathol 119:365–374. https://doi.org/10.1007/s00401-009-0605-1
77. Tsai KJ, Yang CH, Fang YH, Cho KH, Chien WL, Wang WT et al (2010) Elevated expression of TDP-43 in the forebrain of mice is sufficient to cause neurological and pathological phenotypes mimicking FTLD-U. J Exp Med 207:1661–1673. https://doi.org/10.1084/jem.20092164
78. Vatsavayai SC, Yoon SJ, Gardner RC, Gendron TF, Vargas JN, Trujillo A et al (2016) Timing and significance of pathological features in C9orf72 expansion-associated frontotemporal dementia. Brain 139:3202–3216. https://doi.org/10.1093/brain/aww250
79. von Economo C (1926) Eine neue art spezialzellen des lobus cinguli und lobus insulae | SpringerLink. Zeitschrift für die gesamte Neurologie und Psychiatrie 100:706–712. https://doi.org/10.1007/BF02970950
80. Vucic S, Kiernan MC (2006) Novel threshold tracking techniques suggest that cortical hyperexcitability is an early feature of motor neuron disease. Brain 129:2436–2446. https://doi.org/10.1093/brain/awl172
81. Wainger BJ, Kiskinis E, Mellin C, Wiskow O, Han SS, Sandoe J et al (2014) Intrinsic membrane hyperexcitability of amyotrophic lateral sclerosis patient-derived motor neurons. Cell Rep 7:1–11. https://doi.org/10.1016/j.celrep.2014.03.019
82. Walker AK, Spiller KJ, Ge G, Zheng A, Xu Y, Zhou M et al (2015) Functional recovery in new mouse models of ALS/FTLD after clearance of pathological cytoplasmic TDP-43. Acta Neuropathol 130:643–660. https://doi.org/10.1007/s00401-015-1460-x
83. Wegorzewska I, Bell S, Cairns NJ, Miller TM, Baloh RH (2009) TDP-43 mutant transgenic mice develop features of ALS and frontotemporal lobar degeneration. Proc Natl Acad Sci USA 106:18809–18814. https://doi.org/10.1073/pnas.0908767106
84. Winton MJ, Igaz LM, Wong MM, Kwong LK, Trojanowski JQ, Lee VM (2008) Disturbance of nuclear and cytoplasmic TAR DNA-binding protein (TDP-43) induces disease-like redistribution, sequestration, and aggregate formation. J Biol Chem 283:13302–13309. https://doi.org/10.1074/jbc.M800342200
85. Xu YF, Gendron TF, Zhang YJ, Lin WL, D'Alton S, Sheng H et al (2010) Wild-type human TDP-43 expression causes TDP-43 phosphorylation, mitochondrial aggregation, motor deficits, and early mortality in transgenic mice. J Neurosci 30:10851–10859. https://doi.org/10.1523/jneurosci.1630-10.2010
86. Yang Y, Halliday GM, Hodges JR, Tan RH (2017) von Economo neuron density and thalamus volumes in behavioral deficits in frontotemporal dementia cases with and without a C9ORF72 repeat expansion. J Alzheimers Dis 58:701–709. https://doi.org/10.3233/jad-170002
87. Zhou J, Greicius MD, Gennatas ED, Growdon ME, Jang JY, Rabinovici GD (2010) Divergent network connectivity changes in behavioural variant frontotemporal dementia and Alzheimer's disease. Brain 133:1352–1367. https://doi.org/10.1093/brain/awq075
88. Zhou J, Seeley WW (2014) Network dysfunction in Alzheimer's disease and frontotemporal dementia: implications for psychiatry. Biol Psychiatry 75:565–573. https://doi.org/10.1016/j.biopsych.2014.01.020